# MATERIALS, TECHNOLOGIES, CONSTRUCTIONS

# “Special purpose materials”

Redakcja naukowa:
dr hab. inż. Andrzej Trytek, prof. PRz

Stalowa Wola 2019

Wydano za zgodą Rektora

O p i n i o d a w c y

dr hab. inż. Janusz Lubas
dr hab. inż. Marek Mróz, prof. PRz

R e d a k t o r  n a c z e l n y

Wydawnictw Politechniki Rzeszowskiej
prof. dr hab. Grzegorz Ostasz

R e d a k t o r  W y d a n i a

dr hab. inż. Andrzej Trytek, prof. PRz

O p r a c o w a n i e  m a t r y c  i  o k ł a d k i

dr inż. Joanna Zielińska-Szwajka
mgr inż. Sylwia Sikorska-Czupryna

*materials, technologies,*
*constructions, testing*



ISBN 978-83-7934-345-4

Ark. wyd. 3,52, ark. druk. 4,00
Oficyna Wydawnicza Politechniki Rzeszowskiej
al. Powstańców Warszawy 12, 35-959 Rzeszów
https://oficyna.prz.edu.pl
Zam. nr 100/19

Table of Contents

**Chapter 1.**

**Justyna KASIŃSKA**[1*]

# RARE EARTH METALS IN DEFENSE INDUSTRY AND METALLURGY

## Abstract

Rare earth metals have gained wide interest in recent decades. Although studied since the 1950s, new areas of application are still being sought. The commercial significance of the rare earths was largely influenced by the economic growth of China, which has one of the largest deposits of these elements in the world and is the leader in the global rare earth production. This article presents the main defense applications of rare earth elements as important materials in the manufacture of electric motors (magnets), communication, control and guidance systems, laser technologies and others. To demonstrate the beneficial effect of rare earth addition on the mechanical properties of metal alloys, the author reviews the results obtained so far for steel modification in the energy sector. It has been shown that the adding of rare earth elements in an appropriate way and in appropriate amounts significantly contributes to alloy microstructural changes and higher strength properties.

**Keywords:**
rare earth metals, defense industry, metallurgy, new technologies

## 1. Rare earth metals – production and applications

The rare earth metals (REMs) are a group of 17 metallic elements that includes 15 lanthanides spanning atomic numbers 57 to 71 plus scandium and yttrium (Fig. 1.1). Based on the electron configuration, the classification proposed by the International Union of Pure and Applied Chemistry (IUPAC) distinguishes between the light-group rare earth elements (LREEs) and the heavy-group rare earth elements (HREEs).

The term rare earth metals or rare earth elements is a misnomer as the REEs are relatively plentiful and account for one seventh of all elements occurring in nature. The "rarity" originates from the fact that they typically occur in compounds, most commonly in carbonates, oxides, phosphates and silicates

[1*] Department of Metal Science and Materials Technologies, Kielce University of Technology, Al. Tysiąclecia Państwa Polskiego 7, 25-314 Kielce, Poland, kasinska@tu.kielce.pl

[1, 2]. The term “lanthanides” reflects high chemical similarity across this group. Until recently the rare earths, in particular cerium, lanthanum, neodymium and praseodymium, were used in the form of cerium mixture (mischmetal) primarily in metallurgical processes. Over the last 30 years, the rare earths have been applied in aviation, aerospace, automobile, electronic and other technologies (Tables 1.1, 1.2). Due to their properties the rare earths are now being incorporated in military technologies and defense weapon systems.

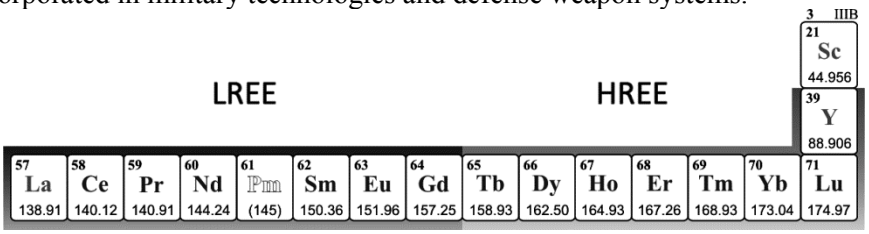

Fig. 1.1. Rare earth elements on the periodic table [3]

Table 1.1. Top areas of REE application, acc. to [4]

| Element | Area of application |
|---|---|
| Scandium, Sc | High-strength Al-Sc alloys, electron beam tubes |
| Yttrium, Y | Capacitors, phosphors, microwave filters, glasses, |
| | radars,lasers, superconductors, lambda sensors |
| Lanthanum, La | Glasses, ceramics, car catalysts, phosphors, |
| | batteries, pigments |
| Cerium, Ce | Polishing powders, ceramics, phosphors, glasses, |
| | catalysts, pigments, mischmetal, UV filters |
| Praseodymium, Pr | Ceramics, glasses, pigments |
| Neodymium, Nd | Permanent magnets, catalysts, IR filters, pigments for |
| glass, lasers | |
| Promethium, Pm | Sources for measuring devices, miniature nuclear |
| | batteries, phosphors |
| Samarium, Sm | Permanent magnets, microwave filters, nuclear industry |
| Europium, Eu | Phosphors |
| Terbium, Tb | Phosphors |
| Dysprosium, Dy | Phosphors, ceramics, nuclear industry |
| Holmium, Ho | Ceramics, lasers, nuclear industry |
| Erbium, Er | Ceramics, dyes for glass, optical fibers, lasers, nuclear |
| industry | |
| Ytterbium, Yb | Metallurgy, chemical industry |
| Lutecium, Lu | Single crystal scintillators |
| Thulium, Tm | Electron bean tubes, visualization of images in medicine |
| Gadolinium, Gd | Visualization of images in medicine, optical and magnetic |
| detection, ceramics, glasses, crystal scintillators | |

Table 1.2. REE application areas acc. to [3]

| Group | Market share [%] |
|---|---|
| Metallurgy | 29 |
| Electronics | 18 |
| Chemical catalysts | 14 |
| New technologies, incl.<br>- display screens,<br>- radars,<br>- lasers. | 12 |
| Automobile catalysts | 9 |
| Polishing powders for glass and ceramics | 6 |
| Permanent magnets | 5 |
| Catalysts for petroleum refining | 4 |
| Other | 38 |

The rare earth metals gained attention about 30 years ago and the demand for these materials has grown recently with the emergence of new sophisticated technologies. It has been estimated that the global production of rare earths will increase by about 40% over the next several years [5]. Table 1.3 compiles annual production of strategic materials such as copper, crude steel and rare earth metals mined at a few dozen to several hundred tons a year, the output which is not commercially significant compared to other assets.

The production of REMs is most advanced in China whose economic rise between 2011 and 2016 created substantial advantages. In North America, economic problems caused most mines to close and affiliated mines in South America to stop or significantly limit production. China is a top global producer, providing as much as 97% global output of REEs (the market worth roughly

**$1.2 billion)** [6] and a top global consumer. Key REM producers and consumers are summarized in Figure 1.2 [7].

Table 1.3. Annual world production of basic metals acc to [7]

| Annual World Production – Comparison [tones] | | | |
|---|---|---|---|
| Crude Steel | 720 Mln | Ind | 600 |
| Copper | 15 Mln | Gal | 100 |
| Lead | 12 Mln | Tellur | 180 |
| Silver | 25 500 | Hafn | 65 |
| Gold | 2 500 | | |

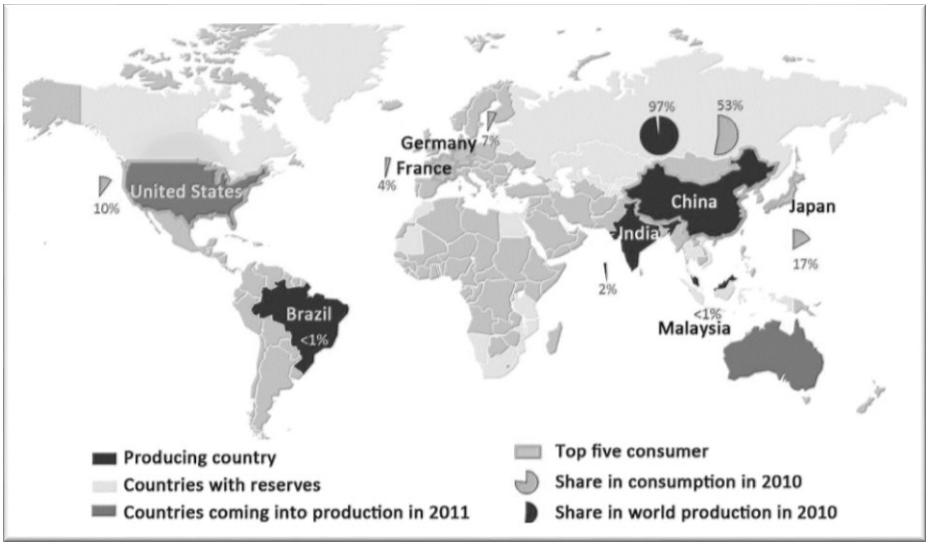


Fig. 1.2. Top producers and consumers of REEs, acc to [7].

At the same time, the use of rare earth elements brings with it a considerable problem of extraction-related environmental degradation. Mining and refining rare earth metals is highly toxic. Excessive rare earth mining has caused landslides, serious accidents, and disasters leading to enormous damage to the safety and health of people and the environment. According to the statistics conducted in Baotou, the primary production site in China, all companies involved in the extraction and separation of the elements into pure metals produce about ten million tons of wastewater annually, and most of this wastewater is discharged without effective treatment. In addition, every ton of rare earths produces 2,000 tons of mining waste, which often contains radioactive elements like thorium. This was a major factor in the failure of Western producers, who

were subject to much stricter environmental standards than those binding in China. In light of this, is renewable energy (solar, wind, electric vehicles) produced with rare earths still "green" [3]?

## 2. Rare earth metals in defense and military applications

Rare earth elements (SmCo, NdFeB) are central to the production of permanent magnets. NdFeB magnets are considered the world's strongest permanent magnets and are essential to many military weapons systems. SmCo retains its magnetic strength at elevated temperatures and is ideal for military technologies such as precision-guided missiles, smart bombs, and aircraft. The superior strength of NdFeB allows for the use of smaller and lighter magnets in defense weapon systems.

Figures 1.3-1.7 [8-10] show the use of rare earth elements in a variety of defense-related applications:

- missile guidance and control systems;
- disk drive motors installed in aircraft, tanks, missile systems, and command and control centers;
- lasers;
- satellite communications, radar, and sonar on submarines and surface ships;
- optical equipment and transducers.

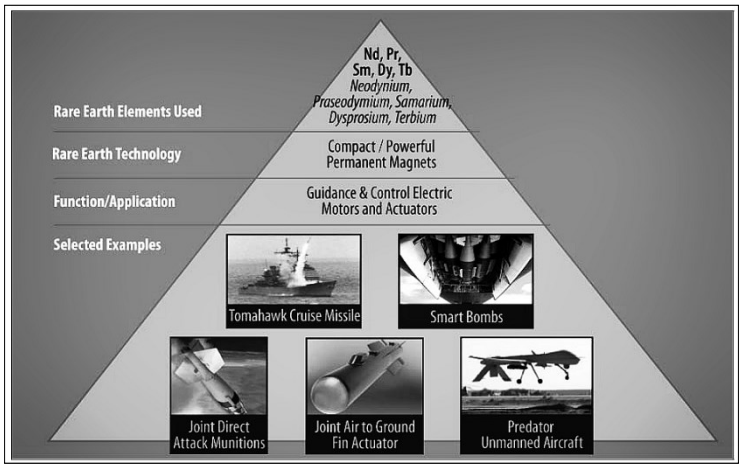


Fig. 1.3. REE in guidance and control systems acc. to [8].

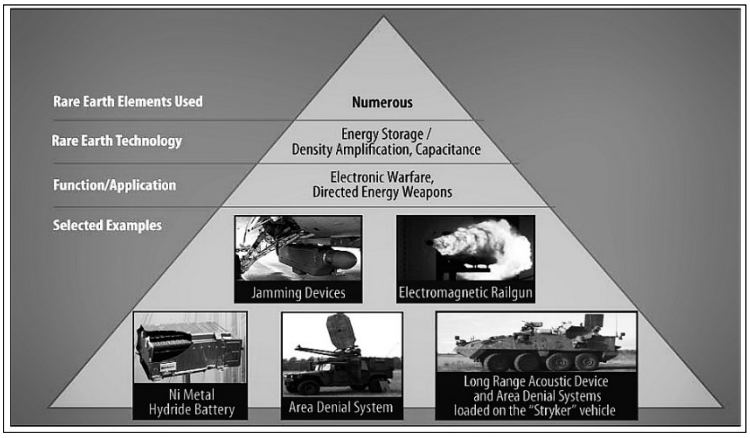


Fig. 1.4. REE in defense electronic warfare acc. to [8].

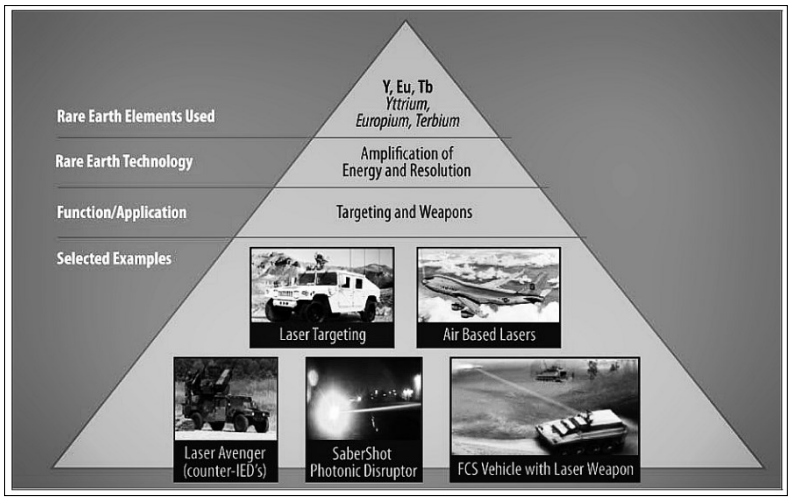


Fig. 1.5. REE in targeting and weapon systems acc. to [8].

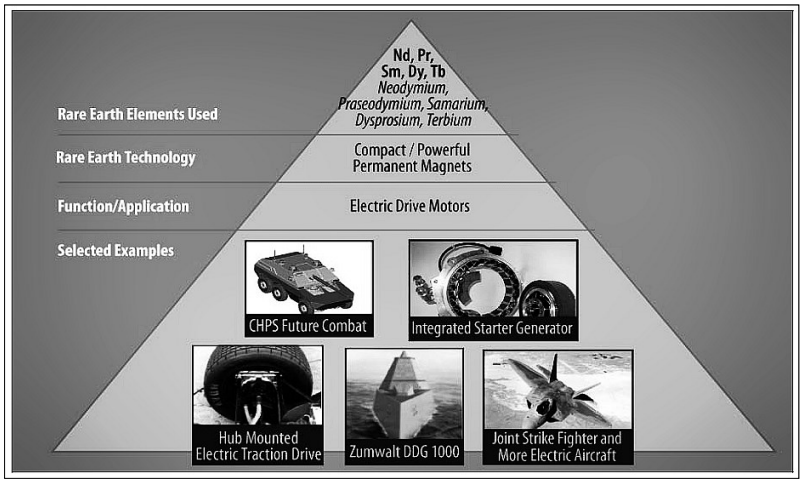


Fig. 1.6. REE in electric motors acc. to [8].

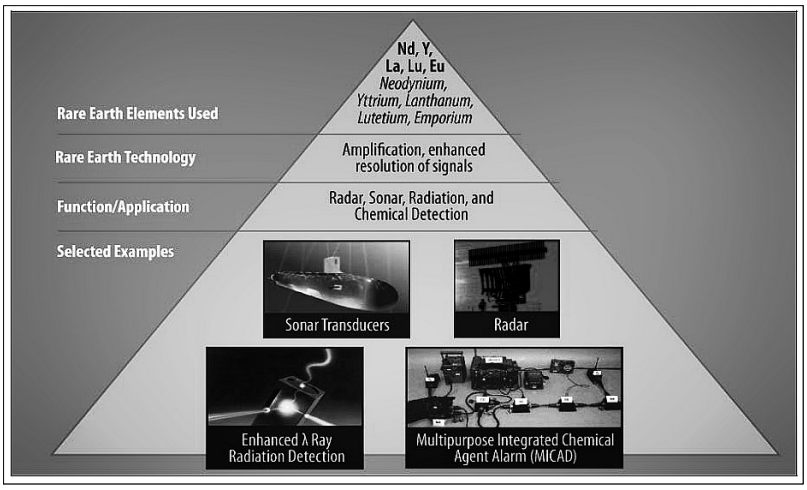


Fig. 1.7. REE in communication acc. to [8].

Military applications of rare earths are briefly described below:

- **Radar and sonar** used to prevent collisions, for surveillance and navigational aids. The Patriot Missile Air Defense System employs radio frequency circulators to magnetically control the flow of electronic signals in the radar and missiles. Rare earths required: gadolinium, samarium, yttrium.

- **Communications and displays required by soldiers,** sailors and airmen to see analog and digital data. Examples are lasers that help line-of-sight communication links in satellite and ground-based systems; old and new computer monitors; and avionics terminals. Rare earths required: dysprosium, erbium, europium, neodymium, praseodymium, terbium and yttrium
- **Lasers employed on vehicle-mounted systems like tanks and armored vehicles**. They can identify enemy targets up to 22 miles. According to DefenseMediaNetwork, "The laser-equipped computer main gun sight on the Abrams M1A/2 tank combines a Raytheon rangefinder and integrated designator targeting system used to obtain a high-probability first hit." Rare earths required: europium, neodymium, terbium and yttrium.
- **Precision-guided munitions (PGMs)** take in a number of missile classes including cruise, anti-ship (ASM) and surface-to-air (SAM), as well as bunker busters. The heat-seeking AIM-9 Sidewinder missile has four fins on its fuselage that use rare-earth magnets to control its flight trajectory. Rare earths required: dysprosium, neodymium, praseodymium, samarium and terbium**.**
- **Guidance and control systems** that steer missiles and bombs towards their targets. Rare earths required: terbium, dysprosium, samarium, praseodymium and neodymium.
- **Electronic warfare** refers to a range of equipment that includes high-capacity power sources, storage batteries and electronic jamming devices. Rare earths required: yttrium-iron-garnet.
- **Electric motors** that require permanent magnets, of which the US Military is an important buyer. New equipment requiring powerful permanent magnets in the next generation of electric motors will include the US Navy's Zumwalt DDG 1000 guided military destroyer, hub-mounted electric traction drives and integrated starter generators. Rare earths required: terbium, dysprosium, samarium, praseodymium and neodymium.
- **Jet engines.** The rare earth element erbium is added to vanadium to make it more malleable for use in vanadium-infused steel that goes into jet engines. While not specifically a rare earth element, the rare element rhenium is alloyed with molybdenum and tungsten. The F-22 Raptor and the F-35 Lightning II stealth fighter reportedly use 6% rhenium in their engines. The electrical systems in aircraft employ samarium-cobalt permanent magnets to generate power.

## 3. Rare earth metals in metallurgy

In modern metallurgical processes, the microstructure of melts is improved at the stage of steel smelting by reducing the degree of macro-segregation, micro-segregation, and changes in dendrite growth kinetics [11]. According to

A. Ghosha, calcium and rare earth metals can be used as refining agents [12] to obtain equiaxed dendrites.

Belyakowa et al. used cerium in the form of Fe-Ce in 40KhNMA steel (0.39% C, 0.76% Cr, 1.60% Ni, 0.20% Mo) and found that the addition of cerium into an ingot mold or ladle reduced the growth rate of austenite grains and affected the change in the number, shape, and type of non-metallic inclusions [13].

Rare earth metals change the morphology of carbides in steels. Hanguang et al. [14] checked the effect of the modifier consisting of 23.53% Ce, 41.78% Si and the balance being Fe on Fe-V-W-Mo steel. They found that in the modified steel after heat treatment, most of the eutectic carbides underwent spheroidization and were more evenly distributed in the matrix. In unmodified steel, carbides were larger in size and were found at the grain boundaries (Fig. 1.8).

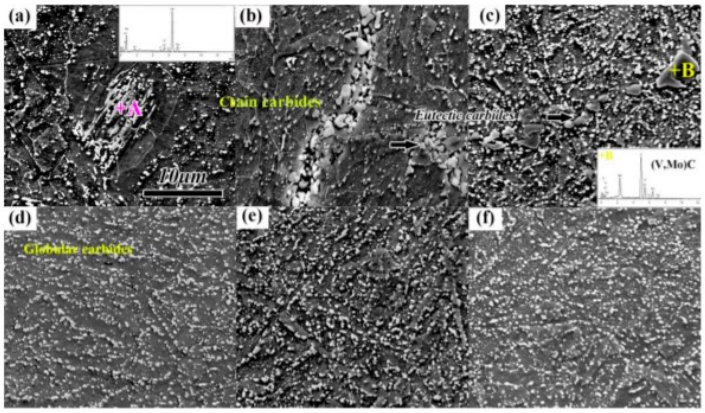


Fig. 1.8. Morphology of carbides, a - carbides aggregation in 0RE, b – chain carbides in 0RE, c – eutectic carbides in 0RE, d- ellipsoid carbides in 0.018RE, e – ellipsoid carbides in 0.048RE, f – ellipsoid carbides in 0.15RE, SEM, EDS.

Rare earth metals affect the crystal structure of metals and alloys through the influence on their mechanical properties.

The author of this work demonstrated the increase in fracture toughness of GP240GH and G17CrMo5-5 cast steels (Fig. 1.9) [15] and showed a reduction in the grain size and a change in the morphology of non-standard inclusions after the introduction of rare earths into the liquid metal (Figs 1.10 and 1.11) [2].

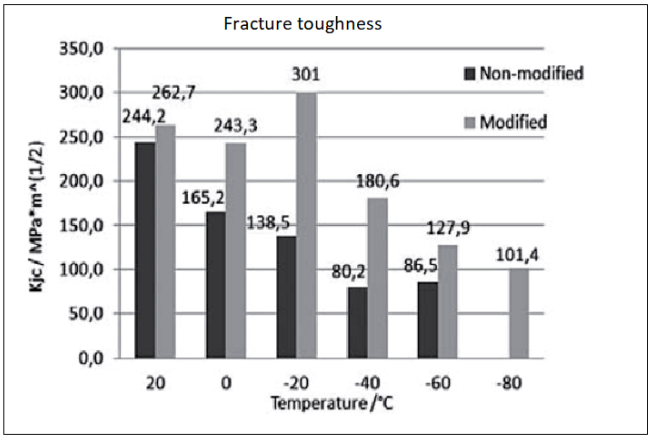


Fig. 1.9. Fracture toughness, $K_{jc}$ for G17CrMo5-5 cast steel [15].

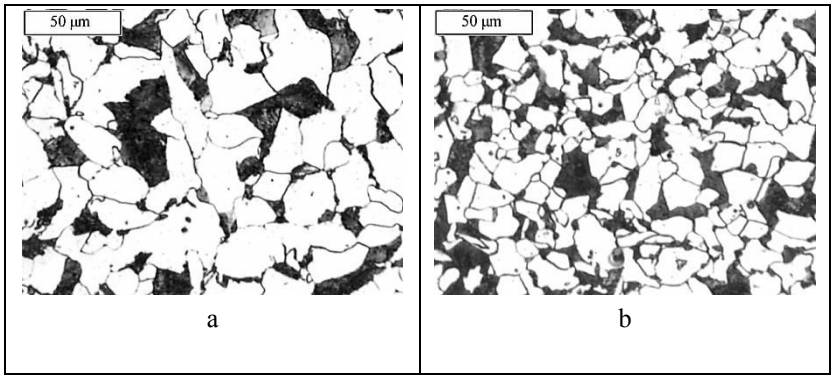


Fig. 1.10. The microstructure of GP240GH cast steel, a non-modified, b – modified, LM.

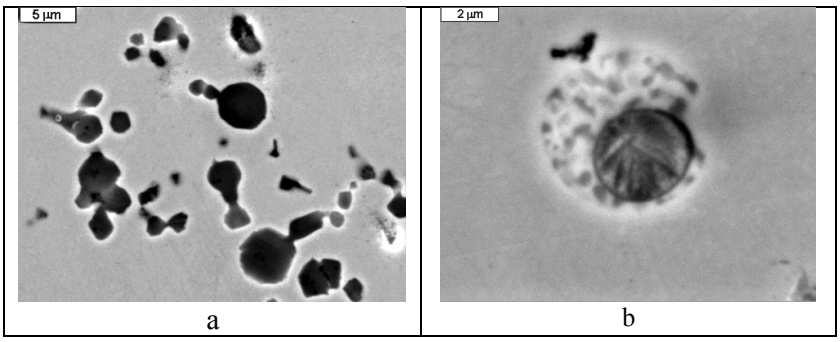


Fig. 1.11. Non-metallic inclusions in non-modified cast steel (a) and in modified cast steel (b).

In addition to the change in the carbide morphology, Minija Wang et al. [16] also reported an increase in tensile strength. They found that rare-earth metals not only contributed to desulphurization of steel, but also removed impurities at the grain boundaries, thus increasing tensile strength up to certain REM quantity limit. The strength decreased when this limit was exceeded. Similar response was observed for impact toughness. In non-modified steel, fracture initiated mainly at the grain boundaries. The most favorable increase in impact toughness was at 0.08% REM content in the alloy. The fracture energy initiation and growth increased by about 50%. Fracture energy increased with increasing REM content in the alloy, but the impact toughness was significantly reduced below the initial values.

Chaus [17] reported similar findings for the modification of high-speed steel with tungsten and molybdenum. By modifying the steel with the Fe-Ce alloy and the Si-MZR mischmetal, he obtained the dendritic structure refinement and an increase in the eutectic carbides' contents through their increased dispersion. As a result, the impact strength rose from 0.10 to 0.16 $MJ/m^2$, with a minimum hardness loss after heat treatment (annealing). Based on the observations reported in [18-20], Chaus claimed that REM increased the number of crystal nucleation sites by dispersing non-metallic inclusions in the matrix and that they constituted a barrier to grain growth [21]. Additional benefits of the modification included the increase in wear resistance and heat resistance of the steel.

The change in the morphology of carbides exerts a significant influence on the properties of steel, as confirmed by Hanguang Fu et al. [14]. Addition of cerium (0.09%) to cast steel consisting of 2.12 - 2.15% C, 4.87 - 4.99% V, 5.18 - 5.19% Cr, 4.83 - 4.99% W, 5.08 - 5.15% Mo, 2.03 - 2.06% Co, and 3.07 - 3.10% Nb increased the refinement of carbides, the hardness, and the fracture toughness in the modified alloy. The authors observed a cleavage fracture on surfaces from non-modified steel specimens. The fractures along the grain boundaries were caused by the formation of carbides at those locations. In the modified steel, ductile transgranular failure predominated.

Wang R.M et al. [22] investigated the influence of lanthanum and yttrium on the properties of high-alloy steel containing nickel, cobalt, niobium, and titanium. Their findings point to the particular deoxidising ability of these elements and significant grain refinement, which, as they claimed, resulted in increased resistance to fatigue fracture, especially after adding yttrium.

Effects of rare earth metals on mechanical properties were investigated by Gladkikh et al. [23], who performed tests on laboratory and industrial heats of nine steels, adding rare earth metals in various forms, such as ferro-cerium, cerium mischmetal, lanthanum, neodymium, and lanthanum oxides. The test temperature for mechanical properties testing was -196 to + 900ºC. They found a sulfur content reduction up to 27% in 15KhGSN2M steel. Non-metallic inclusions occurred in larger quantities in modified steels, however, they had

significantly smaller sizes. The most beneficial effect of REM on the morphology of non-metallic inclusions was observed when they were added at 0.15 - 0.20% [24]. In the case of 50G, 80KP and 09G2 steels, the addition of lanthanum and neodymium did not have a significant effect on the properties at temperatures -196 to +18ºC. At higher temperatures, a slight increase in plasticity was observed. The REM addition lowered the temperature of the transition into brittle state. The increased impact toughness and strength resulted from the reduction in the content of harmful impurities (S, O2, N2, H2) in the steels. The authors also found that the REM content of more than 0.20% had a negative effect on the properties of steel.

The reduction of impurities in the process of steel modification with REM was confirmed by Kang S.K. and Gow K.V. [25] in their studies of carbon steel consisting of 0.70 – 0.72% C, 0.12% Si, and 0.72 – 0.74% Mn, with a cerium content of 0.06%, and a lanthanum content of 0.04%. The researchers observed reduced grain size and a change of MnS sulfides into sulfides or oxysulfides of REM. No significant changes in tensile strength or yield stress were found, and the values of hardness of non-modified and modified steel were not significantly different. But impact toughness increased markedly, which the researchers interpreted as a result of changes in non-metallic inclusion morphology and elimination of anisotropy after hot working.

The influence of structural changes on mechanical properties was investigated by Aksel'rod et al. [26]. They added alkali metals and cerium mischmetal to 20GFBL steel and found that in all the heats the ductile fracture areas were comparable. No changes were found in brittle fracture. Sulfides seen on the unmodified steel fracture surfaces were irregular with sharp edges. In steels after modification, they were globular. Additions of both alkaline earths and rare earths increased fracture energy and the resistance to nucleation and thermal fatigue.

A positive effect of inclusions after their morphology changed due to modification was reported by Kryakovskii et al. [27]. An addition of 0.5 – 3.0 kg cerium mischmetal per ton of steel increased impact toughness, lowered the brittleness threshold in 12Kh1MF steel and improved ductility and impact toughness of 12KhN3A steel.

Similar study was carried out by Belyakova et al. [13]. They observed that the addition of REM to 40KhNMA steel increased impact toughness of sheet metal specimens taken in transverse and longitudinal directions. The change in type and shape of non-metallic inclusions was found to be the responsible for the improvement observed.

The influence of yttrium on the cast steel impact strength was investigated by Volchok et al. [28]. The authors reported that at yttrium content of 0.04 - 0.08%, all the precipitates assumed a spherical shape, and the sulfur content decreased from 10 to 20%. At higher contents of yttrium, phase precipitates were formed at the grain boundaries. The addition of yttrium 0.04 - 0.12% led to a four-fold

increase in the impact toughness of 09GL and 20G2SL steels and an increase in fracture toughness at lowered temperatures. The ductility of steel also increased, but only at 0.04 to 0.05% content of yttrium addition. This increased fracture toughness was interpreted as resulting from the shape change of non-metallic inclusions to spherical.

Xiang and YanXiang [29, 30] modified high-silicon steel (0.76 – 0.77% C, 2.36 – 2.37% Si, 0.36 – 0.38% Mn, 0.27 – 0.29% Mo) with titanium, vanadium, and REM. The yield strength and strength of the steel were found to decrease with increasing temperature of isothermal quenching. A positive effect of modification was observed through the increase in impact toughness, which was 10% at the test temperature of 20ºC, and about 40% at the test temperature of 385ºC.

Improved mechanical properties of 15Kh1M1F steel at the cerium content of 0.1 – 0.15% were reported in [31]. The best results were obtained when cerium addition was made in the ladle or molten steel before smelting ended. Adding ferro-cerium together with calcium silicon and ferrosilicon had a better effect on the formation of non-metallic inclusions. The best effect was obtained when ferro-cerium was added at bath temperatures 1500 – 1590ºC, and when the metal was kept in the ladle for no longer than 25 minutes.

In [27] the researchers discussed the effect of REM on non-metallic inclusions in 30KhGSA, 12Kh1MF and 13KhN3A steels. It was found that REM changed the morphology and distribution of non-metallic inclusions in the steel, which had a positive effect on the mechanical properties. It was also found that the REM addition greater than 0.8 – 1.0 kg per ton of molten metal could lead to macrodefects in those steels due to aggregation of rare earth element inclusions.

Because of close affinity for sulfur, REM additions change the structure, chemical composition, and morphology of sulfides in steels. According to Aksel'rod et al., the sulfides form compounds not only with Ce and other rare earth elements, but also have significantly higher contents of Mn, and its content in sulfides is dependent on the amount and type of the modifier.

Similar observations from modifying high-chromium steel were reported in [32]. In the alloys subjected to modification, sulfide morphology changed to more spherical and formed $RE_2S_3$ or $RE_2S_2O$ precipitates. The authors found that even a small amount of mischmetal up to 0.067% in duplex steel with a 25% chromium content reduced the grain size and amount of $(Mn,Cr,RE)_2S_2O$ type oxysulfides, thus improving corrosion properties of the steel. However, further increase in the amount of REM resulted in a change to more elongated sulfide shapes.

Luniov V.V. [33] claims that the benefits from REM additions in cast steel are due to increased purity of grain boundaries, which leads to better plasticity and elasticity.

REM-induced changes in the microstructure of alloys and morphology of non-metallic inclusions have a range of positive effects, including the improvement

of mechanical properties. As indicated by the research discussed above, REM additions can produce a range of different results.

## 4. Summary

Owing to their unique properties, rare earth metals will have more and more areas of application. For geopolitical reasons, they are and will remain a valuable and sought-after raw material. Their expensive production will still require new technologies in the field of extraction metallurgy and production-related pollution management. A huge advantage of rare earth elements is their use in small quantities (1-2 kg per ton of liquid metal), which reduces production costs markedly. Due to the development of production and research methods, the rare earth elements are expected to remain in the focus of interest of scientists and technologists over the next decades.

## References


[1] Hobart M.King, REE- Rare Earth Elements and their uses, https://geology.com/articles/rare-earth-elements/

[2] Kasińska Justyna (*2011*), Rozprawa doktorska: *Rola wtrąceń niemetalowych w procesie pękania staliwa GP240GH i G17CrMo5-5 modyfikowanego mischmetalem*

[3] Eni Generalic (2012), Rare Earth Elements, https://www.periodni.com/rare_earth_elements.html

[4] Gupta C.K. (2004), Krishnamurthy N.: Extractive Metallurgy of Rare Earths, CRC Press, USA, s.1 – 484

[5] (2017) Metale ziem rzadkich – marginalizowane aktywo, Niezależny Portal Finansowy, https://wmeritum.pl/metale-ziem-rzadkich-marginalizowane-aktywo/189318

[6] Gołyś T. (2010), Metale ziem rzadkich - czysty zysk dla inwestora i skuteczna broń Chin, https://forsal.pl/artykuly/461946,metale-ziem-rzadkich-czysty-zysk-dla-inwestora-i-skuteczna-bron-chin.html

[7] https://independenttrader.pl/metale-ziem-rzadkich-marginalizowane-aktywo.html?sort=latest

[8] Valerie Bailey Grasso (2013), Rare Earth Elements in National Defense: Background, Oversight Issues, and Options for Congress, December 23

[9] USGS Fact Sheet 087-02, and USGS Mineral Commodity Summaries, January 2010, http://pubs.usgs.gov/fs/2002/fs087-02/

[10] Ratnam, Gopal. Rare Earth Shortage Would Spur Pentagon to Action. Bloomberg News , April 9, 2012, http://www.bloomberg.com/news/2012-04-09/rare-earths-shortage-would-spur-pentagon-to-action.html.

[11] G. Ruizhen, C. Xiaoguang (1985), Influence of REM on micro – segregation in cast steel, Proc. 1st International Steel Foundry Congress, pp.201 – 208

[12] I.P. Volchok, A.V. Tsarev, V.P. Rudenko (2004), Raising the impact strength of cast steel by modification with yttrium, *Materials Science*, p 586 – 587

[13] A.F. Belyakova, Yu.V. Kryankovski, I.V. Paisov (1996), *Effect of rare earth metals on the structure and properties of structural steel*, Metal Science and Heat Treatment, **7**, No 9, p 588 – 593

[14] Hanguang Fu, Qiang Xiao, Yanxiang Li (2005), *A study of the microstructures and properties of Fe-V-W-Mo alloy modified by rare earth*, Materials Science and Engineering A, 395, p 281 – 287
[15] J. Kasińska (2016), *Modification influence of mischmetal on fractography fracture of G17CrMo5-5 cast steel samples after the three-point bending test*, Metalurgija, 55 (4), p 749-752
[16] W. Mingjia, M. Songmei, S. Feifei, W. Yan (2007), *Influence of rare earth elements on microstructure and mechanical properties of cast high-speed steel rolls*, Journal of Rare Earths, 25, p 490 – 494
[17] A.S. Chaus (2004), *Use of REM-based modifying agents for improving the structure and properties of cast tungsten-molybdenum high-speed steels*, Metal Science and Heat Treatment, 46, p 415 – 422
[18] V. Paisov, Yu A. Bashnin, G.V. Semenchenko (1968), *Effect of REM on the structure and properties of high-speed steel R9*, Izv. Vuzov, Chern. Met.,7, p 124 – 128
[19] N. Jamanchi, K Sudo (1986), *The effect of rare earth element additions on the properties of the SKH-51 high-speed steel*, Electric Furnace Steel, 57(3), p 167 – 169
[20] Y.U. Tamura (1988), *The effect of rare earth element additions on the structure after crystallization on the W – Mo high-speed steel, alloyed by 3% V*, Cur. Adv. Mater. Proc., No. 1
[21] A.S. Chaus, F. I. Rudnitskii (1989), *Effect of modifying on the structure and properties of cast tungsten-molybdenum highspeed steels,* Metalloved. Term. Obrab. Met., , 2, p 27 – 32
[22] R.M. Wang, Y.G. Song, Y.F. Han (2000), *Effect of rare earth on the microstructures and properties of a low expansion superalloy*, Journal of Alloys and Compounds, 311, p 60 – 64
[23] A.N. Gladkikh, V.N. Gurashov, V.A. Skudnov, L.D. Sokolov (1970), *Mechanical properties of commercial steels with rare – earth metals*, Metallovedenie I Termicheskaya Obrabotka Metallov, 3, p 31 – 34
[24] V.N. Gurashov and all (1968), Increasing the Quality of Steels and Alloys by Alloying with Rare - Earth Metals, Kijów – Odessa
[25] S.K. Kang, K.W.Gow (1979), *Mechanical Properties of Rare Earth Metal Treated Rail Steels*, Metallurgical and Materials Transactions A, 10, No. 11, p 1800 – 1802
[26] A.E. Aksel'rod, V.V. Popov, A.F. Filippenkov (1988), *Effect of alkaline and rare earth metals on the composition of sulfide inclusions and properties of cast steel*, Metal Science and Heat Treatment, 30, No 12, p 931 – 935
[27] Yu.V.Kryakovskii, Yu.I. Rybenchik, E.I. Tyurin, V.I. Yavoiskii (1963), *Mechanical properties and the nature of nonmetalic inclusions in structural steel containing rare earth elements*, Metal Science and Heat Treatment, 5, p 432 – 439
[28] I.P. Volchok, A.V. Tsarev, V.P. Rudenko (2004), *Raising the impact strength of cast steel by modification with yttrium*, Materials Science, p 586 – 587
[29] CH. Xiang, L Yanxiang (2006), *Effect of Ti, V and Rare Earth on the Mechanical Properties of Austempered High Silicon Cast Steel*, Metallurgical and Materials Transactions A, 37A, p 3215 – 3220

[30] CH. Xiang, L. Yanxiang (2007), *Fracture toughness improvement of austempered high silicon steel by titanium, vanadium and rare earth elements modification*, Materials Science and Engineering A, 444, p 298 – 305
[31] N.S. Kreshchanovskii, V.R. Nazarenko, G.A. Ryzhkova (2004), *Effect of cerium on the mechanical properties of 15Kh1M1F steel*, Metal Science and Heat Treatment, 07, p 444 – 448
[32] Yo.H. Heong, P. Chan Jin, K. HyukSang (2006), *Effects of misch metal on the formation of non-metallic inclusions and the associated resistance to pitting corrosion in 25%Cr duplex stainless steels*, Scripta Materialia, , 55, p 991 – 994
*[33]* V.V. Luniov (2003), *Wtrącenia niemetaliczne a właściwości staliwa, Przegląd Odlewnictwa*, , 59, p 299 – 304 (*Non-metallic inclusions and properties of cast steel*, Foundry Journal of the Polish Foundryman'a Association)

**Chapter 2.**

**Wojciech PRZETAKIEWICZ**[1]
**Katarzyna BRYLL**[1,*]
**Ewelina KOSTECKA**[1]
**Dorota STOCHŁA**[1]
**Marek STAUDE**[1]

# APPLICATION OF MICROSCOPY IN THE ASSESSMENT OF POROSITY IN COMPOSITE CASTS SATURATED WITH SILUMIN

## Abstract

Composites produced by pressure infiltration are characterized by both a greater number and a larger variety of defects compared with traditional castings. Porosity is a significant disadvantage in such materials, and the pore formation mechanisms are closely related to the production of castings. This paper determines the usefulness of microscopy methods in the examination of porosity on example metal composites saturated with silumin.

**Keywords:**
Composite, metal matrix composite, silumin, porosity

## 1. Introduction

The ideal structure of infiltrated composite castings consists of a metal matrix, typically a commercial alloy based on Al, Mg, or Ti, and a reinforcement material, most often a ceramic, in the form of unstructured fibres that form a system of capillaries with different sizes and shapes (Fig. 2.1).

[1] Department of Marine Engineering Materials, Faculty of Marine Engineering, Maritime University of Szczecin, Willowa 2–4, 71-650 Szczecin, Poland
[*]e-mail: k.bryll@am.szczecin.pl

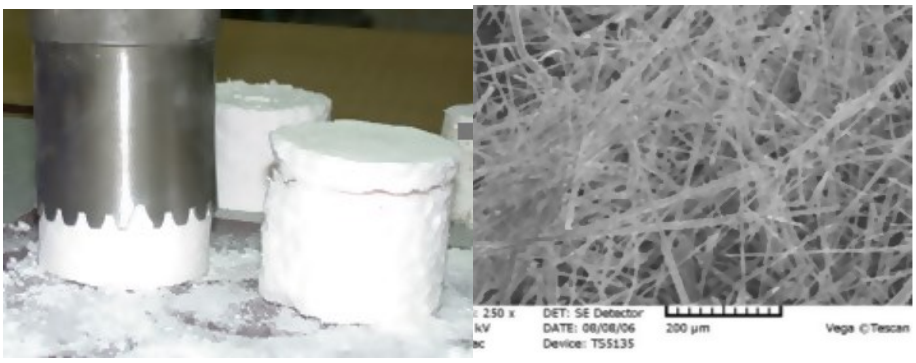


a) b)

Fig. 2.1. Structure of a reinforcing aluminosilicate preform: (a) macroscopic view [1], (b) short unstructured fibre (SEM) [2].

Due to the poor wettability of the reinforcement material by the liquid matrix, the infiltration of a composite reinforcement material is sometimes forced by external pressure. The component properties and the reinforcement infiltration method make it practically impossible to obtain a nonporous saturated composite material [1-5]. Porosity in a composite structure may be caused by [5] insufficient saturation of the composite reinforcement capillaries by the liquid metal matrix, discharge of a gas dissolved in the matrix metal when it cools and solidifies, as well as the formation of gas occlusions during infiltration of reinforcement. Pores can have different shapes and locations in a casting, and their sizes can vary significantly, making it difficult to classify the porosity formation mechanism. Attempts to identify the type of porosity have been presented in various publications [1, 5-8]. The assessment of a composite material's porosity is used to judge its quality, whereas the type of pores makes it possible to determine the causes of their formation, which allows process parameters to be adjusted to minimize the casting's porosity. In addition to densitometry, ultrasound, X-ray, and other methods, microscopy techniques are used to assess the porosity of cast metal composites. In order to detect porosity using microscopy, an appropriate area for analysis must be selected, and pores must be identified by noting a clear distinction between pores and other components of a composite, e.g., impurities or inclusions. It is also important to select the appropriate microscopic technique for the type of reinforcement metal in an infiltrated composite. The quantitative porosity determined for the material tested by microscopic methods is also influenced by the preparation of polished sections, i.e. metallographic specimens (a very complex process which requires experience since metal composites such as those with a soft silumin matrix have a varying hardness due to the presence of hard reinforcement), the selection of appropriate magnifications, and unambiguous interpretation of visible objects. In this paper, the usefulness of various microscopy methods for the identification of porosity of metal composite

materials with different types of reinforcement was determined. After the porosity was unambiguously identified, a quantitative description can be performed.

## 2. Testing of the porosity of metal composites using microscopy

Two types of metal composites were tested in this paper that differed in their reinforcement material. In the first material, composites with a silumin matrix and aluminosilicate reinforcement in the form of short fibres (unstructured and shaped in preforms), were examined. In the second case, composites with a silumin matrix and carbon reinforcement in the form of short, unstructured fibres formed into preforms were investigated. Reinforcement preforms (dimensions of D=60 mm x L=20mm) were introduced into a metal form (the aluminosilicate reinforcement was heated in a furnace at 760 °C for 60 minutes), filled with liquid silumin (AlSi11), and infiltrated at 20 MPa for 300 seconds (Fig. 2.2). All requirements were met for the technology of making castings by infiltration using squeeze casting [3-5].

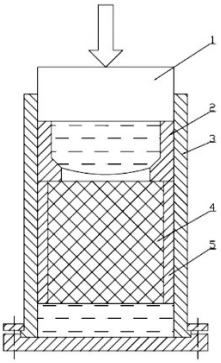


Fig. 2.2. Production of composites by infiltration of a porous structure with a liquid metal matrix: scheme of a mould with a preform prepared for saturation: 1 – stamp, 2 – piston, 3 – bushing, 4 – ceramic preform, and 5 – reinforcement seat.

### 2.1. Testing the porosity of the composite of AlSi11 and aluminosilicate fibres

Non-etched polished specimens were cut from a cast composite of AlSi11 and aluminosilicate fibre and used as samples for microscopic observation. Porosity was examined using a Neophot 2 optical microscope. Attempts were made to digitally process the recorded images (Fig. 2.3a) using Aphelion software [1]. However, the results were not satisfactory (Fig. 2.3b-c). A similar test was carried out for silver-sprayed specimens (Fig. 2.4a), which also returned unsatisfactory results (Fig. 2.4 b-c). For these composites, the use of optical microscopy for

porosity analysis is inappropriate because it is impossible to identify these defects in an unambiguous way. Therefore, to determine the porosity of a composite with an aluminosilicate reinforcement, it was decided to analyse images obtained from a scanning electron microscope (SEM) [1].

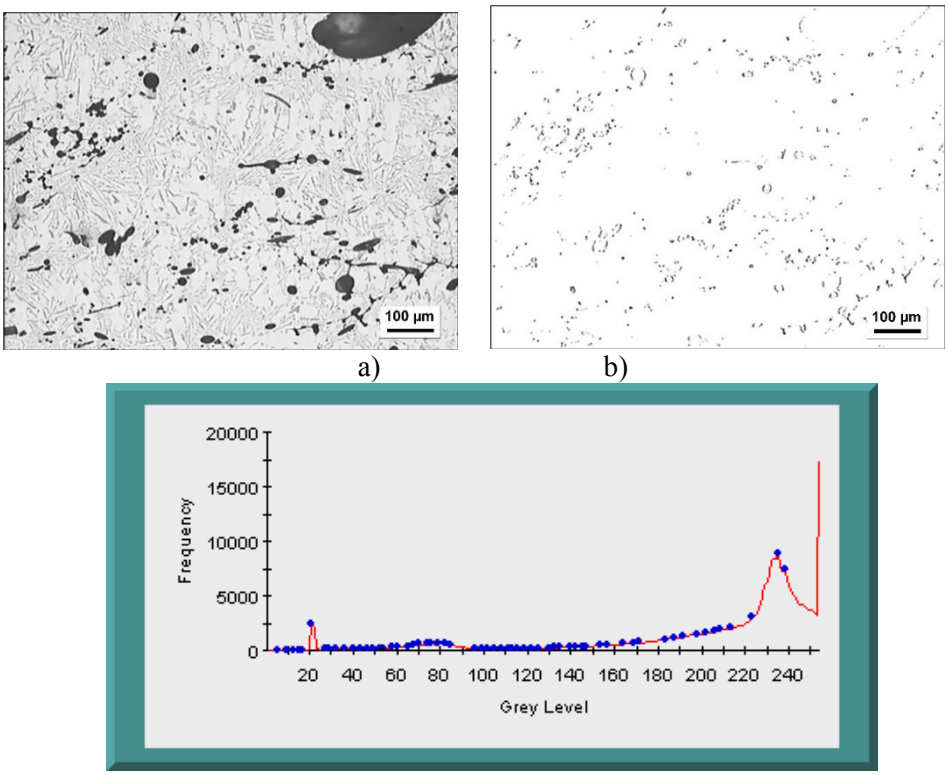


Fig. 2.3. A trial computer-aided analysis of a porosity image (Aphelion software); material: $Al_2O_3/SiO_2$ fibre, AlSi matrix (non-etched specimens); a – output image [1], b – unsuccessful attempt [1], c – grey level histogram.

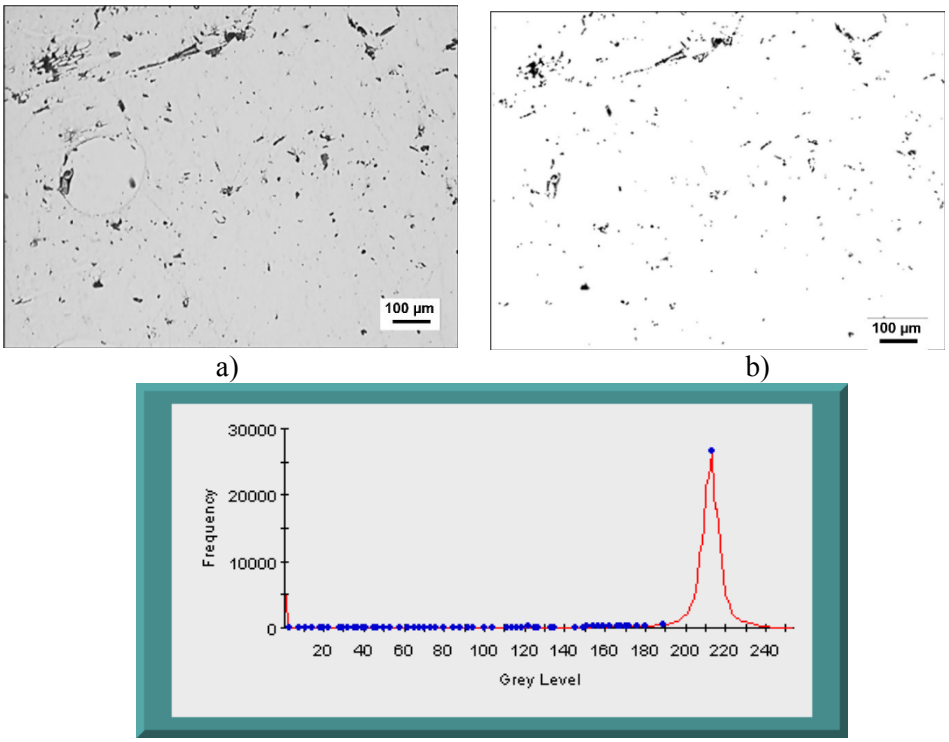


Fig. 2.4. A trial computer-aided analysis of a porosity image (Aphelion software); material: $Al_2O_3/SiO_2$ fibre, AlSi matrix (silver-sprayed sample), area of 225× ; a – output image, b – unsuccessful attempt, c – grey level histogram.

To identify pores, a Philips XL 30 Everhart-Thornley SEM was used, which ensured time-independent, high-quality topographic images of the tested sample surfaces (Fig. 2.5a). The use of the back-scattered electron (BSE) detector allowed differences in the chemical composition or topography of the metallographic specimens being tested to be observed (a "campo" or a "topo" image). This allowed an image to be appropriately transformed and modified (Figure 2.5c). In images processed in this way, a porosity-type defect could be unequivocally identified in this composite (Fig. 2.5d).

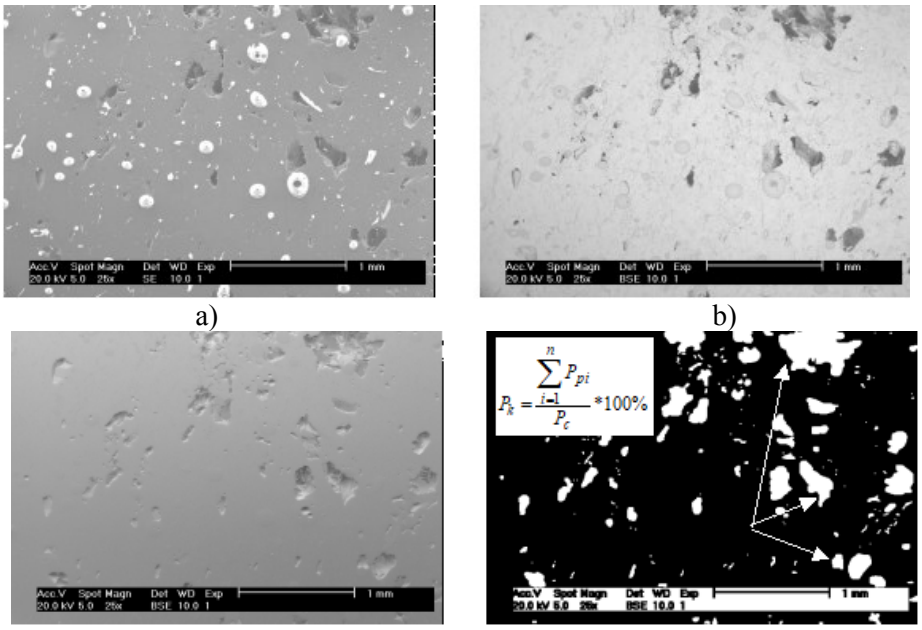


a) b)

c) d)

Fig. 2.5. Example of a tested composite structure view (aluminosilicate reinforcement, AlSi11 matrix); a – SEM image, b – BSE image, c – BSE-TOPO image, d – a scheme for planimetric determination of porosity on a binary image [6].

## 2.2. Testing the porosity of the composite of AiSi11 and carbon fibres

Porosity was detected similarly to composites reinforced with aluminosilicate. The digital images (Fig. 2.6a) were subjected to processing with the Aphelion software. To identify objects, images were modified, and objects to be analysed were filtered out with a specified brightness and colour (Fig. 2.6b).

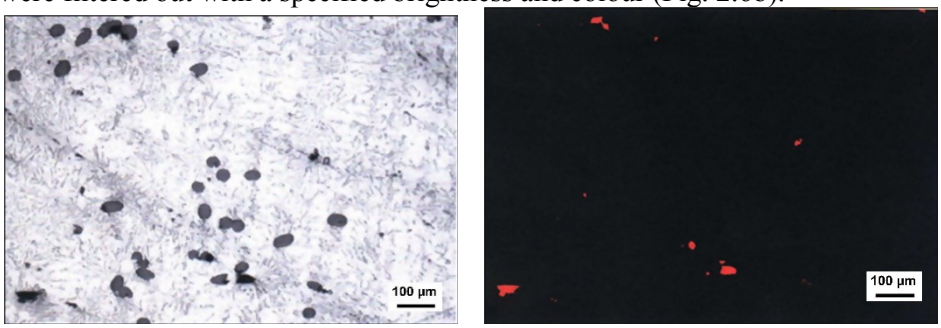


a) b)

Fig. 2.6. Example of porosity analysis: a – analysed area, b – porosity; computer-aided image analysis (Aphelion); composite: carbon fibre reinforcement, AlSi11 matrix; pressure of 20 MPa, optical microscopy.

In this case, there were no difficulties in distinguishing the pores from other elements of the composite. Thus, optical microscopy was determined to be sufficient to examine the porosity in composites of this group.

## 4. Summary

After appropriate computer processing, the image obtained from an optical microscope was sufficient to unequivocally identify a porosity-type defect in the examined surface of composites with a silumin matrix (AlSi11) reinforced with carbon fibre. Since an optical microscope image was not useful for determining the type of porosity of castings made of composites reinforced with aluminosilicate due to the presence of impurities and occlusions in the reinforcement material which may be erroneously interpreted as porosity [8-14], it was necessary to use other microscopy methods to identify pores. The examination of these materials with a scanning electron microscope was not difficult, however, the image must be prepared appropriately. Choosing the proper method to identify a porosity-type defect in the tested composites, depending on the type of reinforcement used, ensures the reliability of the subsequent quantitative assessment of this defect [1, 6, 14-20].

## References


[1] Gawdzińska K. (2003): *Analiza i klasyfikacja wad odlewów z metalowych kompozytów nasycanych*. Praca doktorska, Politechnika Szczecińska,(niepublikowana)

[2] Nagolska D., Gawdzinska K. (2012): *Analysis of impact of reinforcing preforms saturation on selected properties of obtained metal-matrix composite castings.* Archives of Foundry Engineering Vol. 12, iss. 1s, 143-148

[3] Grabian J. (2001): *Nasycanie zbrojenia z ceramicznych włókien nieuporządkowanych podczas wytwarzania odlewów z kompozytów metalowych*. WSM, Szczecinie.

[4] Sobczak J. (2001): *Kompozyty metalowe*. Instytut Odlewnictwa – Kraków, Instytut Transportu Samochodowego – Warszawa

[5] Gawdzińska K., Chybowski L., Przetakiewicz W. (2015): *Proper matrix-reinforcement bonding in cast metal matrix composites as a factor of their good quality*. Archives of Civil and Mechanical Engineering 16(3), 553–563. doi: 10.1016/j. acme.2015.11.004

[6] Jackowski J., Gawdzińska K., Zasada D. (2002): *Ocena zwartości struktury odlewu z metalowego kompozytu nasycanego*. Archiwum Technologii Maszyn i Automatyzacji, vol. 22, nr 1, Poznań

[7] Kaptay G. (2006): *On the equation of the maximum capillary pressure induced by solid particles to stabilize emulsions and foams and on the emulsion stability diagrams*. Colloids and Surfaces A: Physicochemical and Engineering Aspects 282–283, 387–401.

[8] Gawdzińska K., Chybowski L., Bejger A., Krile S., (2016): *Determination of technological parameters of saturated composites based on sic by means of a model liquid*, Metalurgija, Vol. 55 No. 4, s. 659-662, 2016 [ISSN 0543-5846, e-ISSN 1334-2576]

[9] Naplocha K. (2013): *Materiały kompozytowe umacniane preformami wytworzonymi w procesie wysokotemperaturowej syntezy w polu mikrofalowym*. Oficyna Wydawnicza Politechniki Wrocławskiej, Wrocław

[10] Richter J., Krajzel J., (2013): *Nickel-based binding phase effect upon selected properties of supercoarse sintered carbides*, Proceedings of 18th Plansee Seminar, Austria, pp. 1628–1632
[11] Richter J. (2014): *New grades of supercoarse sintered carbides with nickel based matrices*, Report for the National Science Center, Project 222/B/T02/2011/40, Katowice, Poland
[12] Naplocha K., Dmitruk A., Lichota J., Kaczmar J.W. (2016): *Heat transfer in high porosity cellular material – PCM for the energy storage*. The 33rd Danubia-Adria Symposium 148 on Advances in Experimental Mechanics: book of abstracts. Ljubljana: SSEM – Slovene Society of Experimental Mechanics, 136–137
[13] Orłowicz, A.W., Tupaj, M, Mróz, M, Trytek, A. (2015): *Combustion Engine Cylinder Liners Made of Al-Si Alloys*. Archives of Foundry Engineering. 15. 10.1515/afe-2015-0041. Gawdzińska K., Jackowski L., Szweycer M., Odmiany porowatości odlewów z metalowych kompozytów nasycanych, „Kompozyty", Rocznik 1, nr 1, Wyd. Politechnika Częstochowska 2001
[14] Gawdzińska, K., Bryll, K., Nagolska, D. (2016): *Influence of Heat Treatment on Abrasive Wear Resistance of Silumin Matrix Composite Castings*. Archives of Metallurgy and Materials, 61, 1, p. 177–182
[15] Chybowski L., Grządziel Z., Gawdzińska K. (2018): *Simulation and Experimental Studies of a Multi-Tubular Floating Sea Wave Damper*. Energies, 11(4), s. 1012:1-20 [ISSN 1996-1073, DOI: 10.3390/en11041012]
[16] Gawdzińska K., Chybowski L., Nabiałek M., Szymański P. (2019): *A Study of Metal–Ceramic Composite Foams Combustibility*. Acta Physica Polonica A, 135(2), 304-307 [eISSN 1898-794X, ISSN 0587-4246, DOI: 10.12693/APhysPolA.135.304]
[17] Kaczyński P., Ptak M, Fernandes F. A. O., Chybowski L., Wilhelm J., Alves de Sousa R. J. (2019): *Development and Testing of Advanced Cork Composite Sandwiches for Energy-Absorbing Structures*. Materials, 12(5), 697:1-14 [ISSN 1996-1944, DOI: 10.3390/ma12050697]
[18] Gawdzińska K., Bryll K., Chybowski L., Berczyński S. (2018) *The impact of reinforcement material on selected mechanical properties of reinforced polyester composites*. Composites Theory and Practice, R18, nr 2, s. 65-70, [ISSN 2084-6096, online ISSN 2299-128X]
[19] Gawdzińska K., Chybowski L., Przetakiewicz W., Laskowski R. (2017): *Application of FMEA in the Quality Estimation of Metal Matrix Composite Castings Produced by Squeeze Infiltration*. Archives of Metallurgy and Materials, vol. 62 (4), s. 2171-2182, [DOI 10.1515/amm-2017-0320]
[20] Gawdzińska K., Chybowski L., Przetakiewicz W. (2017): *Study of Thermal Properties of Cast Metal-Ceramic Composite Foams*. Archives of Foundry Engineering, Vol. 17(4), s. 47-50

**Chapter 3.**

**Piotr NAWROCKI[1*]**
**Kamil WASILUK[2]**
**Karolina ŁUKASIK[1]**
**Dawid MYSZKA[1]**

# INFLUENCE OF EVALUATED TEMPERATURE OF INTERCRITICAL TREATMENT ON MECHANICAL PROPERTIES OF AUSTEMPERED DUCTILE IRON

## Abstract

Ductile iron with ausferritic matrix obtained as a result of austenitization and then austempering is characterized by a combination of high strength properties along with good wear resistance and good ductility. Austenitisation in intercritical temperatures is described in the literature, but the phenomena associated with the use of this range preceded by austempering in cyclic processing is not fully understood. The paper attempts to evaluate the influence of heat treatment within the intercritical field on the microstructure and properties of austempered ductile iron (ADI) with an increased content of Mo, Ni and Cu elements. The aim of the work was to maximize the fragmentation of the ductile iron matrix microstructure by selecting a low temperature of isothermal transformation, i.e. 40°C above Ms temperature in the lower bainite range. Heat-treated cast iron was subjected to dilatometer tests, microstructure research, hardness and impact tests. It was found that cyclic heat treatment and the use of the intercritical range during austenitizing may affect the strong grain refining of austenitic grain and achieving high fracture toughness.

**Keywords:**
austempered ductile iron (ADI), intercritical temperature, impact properties, dilatometric tests, bainitic transformation.

---

[1] Department of Metal Forming and Casting, Warsaw University of Technology, Narbutta 85, 02-524 Warsaw, Poland
[2] Department of Surface Engineering, Warsaw University of Technology, Wołoska 141, 02-058 Warsaw, Poland
[*]e-mail: p.nawrocki@wip.pw.edu.pl

## 1. Introduction

The best compromise between high strength and good ductility in nodular cast iron is obtained by performing a heat treatment of austempering, consisting of two steps: austenitization above $A_1$ temperature, usually between 820 - 900°C, fast cooling to the temperature within range of 200 – 400°C and isothermal hold in that temperature [1]. As a result, an unique microstructure is formed, consisting of a mixture of high carbon content austenite (γHC) and ferrite plates (α), called ausferrite. This structure can be achieved with proper cooling rate after austenitization to prevent diffusive transformations in inhomogeneous as-cast microstructure [2-3]. Microsegregation of alloying elements often causes necessity of preliminary treatment, ex. normalization or ferritization, especially when treated element has a variable cross-section.

Main parameters of austempering are time and temperature of austenitization and time and temperature of austempering. Increment of austenitization temperature results in higher carbon concentration in austenite which causes better hardenability but also increases total time of ausferritic transformation. Decrement of austenitization temperature increases driving force of austenitic transformation, which can lead to significant refinement of microstructure. Considering the above, austenitization temperature should be minimized to a level sufficient to achieve 1.1 – 1.3 wt.% of carbon concentration in austenite. Temperature of austempering affects the kinetics of ausferritic transformation and morphology of forming microstructure. Austempering within lower range of transformation temperatures results in higher fraction of thin bainitic ferrite plates in final microstructure and, subsequently, lower content of carbon-enriched austenite. The amount of high carbon content austenite in such microstructure is too low to ensure good plasticity while maintaining high strength. Formation of martensite during cooling to low austempering temperature can also occur. With an increment of austempering temperature a decrement of mechanical strength and improvement of plasticity is observed [4]. Numerous studies [5-8] on optimization of ausferritic transformation that have been published often are concentrated on analyzing only a narrow range of austempering temperatures. Recently, a number of papers regarding austenitization in the intercritical zone have been published [9-10]. In paper [9] analyzed series of intercritical austenitizing temperatures ranging from 775 to 900°C with subsequent austempering performed at 300 and 400°C on a conventional unalloyed ductile iron. Reported results showed that all mechanical properties increased with intercritical austenitizing temperatures till an optimum austenitizing temperature of 830°C. At this optimum processing condition, tensile strength of 974 MPa and very high toughness of 166 J was achieved. This paper aims to estimate the influence of prior heat treatment and austenitization within intercritical zone parameters on microstructure and properties of an austempered ductile iron. It is also an attempt to comprehensively solve the problem of selection of

transformation parameters using dilatometric tests, which enable designing standard heat treatment of nodular cast iron, but above all are a starting point for the design of complex processing variants, eg with pre-treatment or intercritical.

## 2. Materials and methods

For the purpose of experiment a database of heat treated ductile cast iron, containing chemical composition, heat treatment, properties and microstructure data from over 100 published papers and own research, was created. Collected data was used to choose chemical composition of a ductile iron, optimal for obtaining good mechanical properties after heat treatment in a variety of different cast modules. Selected chemical composition is shown in table 3.1.

Table 3.1. Chemical composition of ductile iron (wt. %)

| | C | Si | Mn | Ni | Cu | Mg |
|---|---|---|---|---|---|---|
| min. | 3,40 | 2,40 | 0,20 | 1,80 | 0,50 | 0,055 |
| max. | 3,55 | 2,50 | 0,35 | 2,00 | 0,80 | 0,060 |

The material was cast as Y2-shaped standard test blocks by the Foundry Institute in Krakow. Casting were performed in medium frequency induction furnace with loading capacity of 50 kg. The cast batch was composed of special crude iron containing C –4,30 wt.%, Si – 0,40 wt.%, Mn – 0,03 wt.% and steel scrap. Spheroidisation was performed at 1400 – 1420$^0$ C at the vat bottom using FeSiMg9, followed by a modification using FeSi75. Samples for spectrometric analysis were produced (table 3.2) and the melt was casted at 1350°C to bentonite-bounded sand moulds. The microstructure of the obtained ductile iron in the as-cast state is presented in figure 3.1. Based on unetched metalografic samples observation the amount of graphite nodules was estimated to be 11%. The obtained castings were cut into smaller samples (figure 3.2), which were subject to a heat treatment.

Table 3.2. Chemical composition of ductile iron (wt. %)

| C | Si | Mn | Mo | Ni | Cu | Mg |
|---|---|---|---|---|---|---|
| 3,55 | 2,5 | 0,35 | 0,55 | 1,90 | 0,5 | 0,058 |

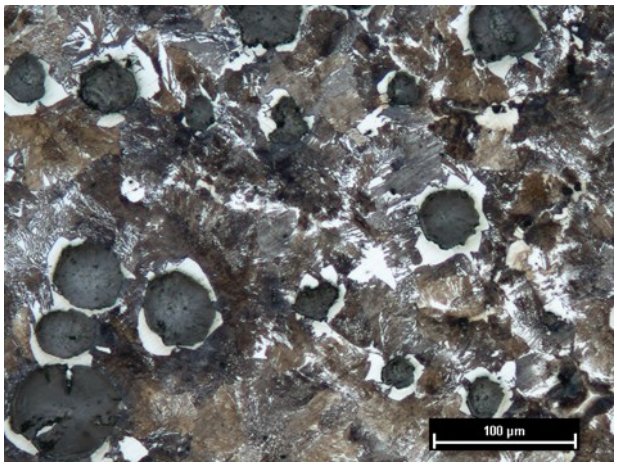


Fig. 3.1. Microstructure of the obtained Mo-Ni-Cu cast iron (etched with nital)

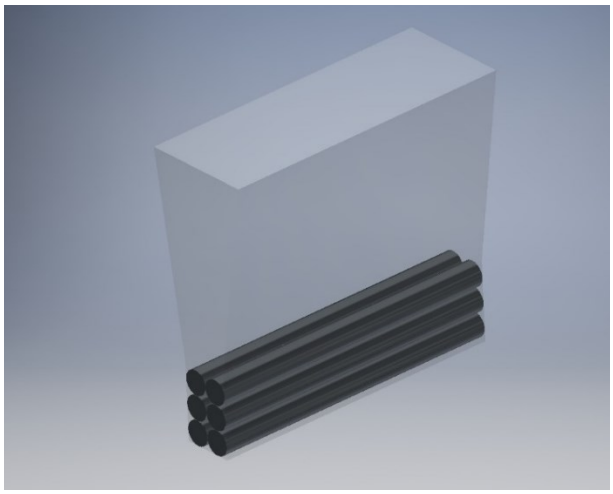

Fig. 3.2. Casting with specimens for heat treatment and dilatometric examinations

Heat treatment parameters for investigated ductile iron were determined after dilatometric study of phase transformation kinetics. Cylindrical samples for dilatometric experiment with diameter of 3 mm and length of 10 mm were cut from Y2 blocks using EDM. Experiments were carried out on Bahr DIL 805 Pro quenching dilatometer. Heat treatment of bulk samples for metallographic and mechanical experiments was conducted in resistant furnace and fluidized bed. Microstructure observation was performed on metallographic samples using an scanning electron microscope JEOL JSM-IT100 scanning electron microscope in

Institute of Precision Mechanics in Warsaw at magnifications in the range of x1000 and x5000. The HRC surface hardness tests were performed using an Wilson hardness tester, performing 3 readings on each of the samples. Charpy impact test was carried out according to EN ISO 148-1_2011 standard using Zwick/Roell Charpy pendulum with impact energy of 300 J. For this test, standard sized 10 x 10 x 55 mm unnotched samples were utilized.

**2.1. Heat treatment**

The first step to design a heat treatment was determination of characteristic temperatures by dilatometric study. Figure 3.3 shows fragment of change of sample's length against temperature plot from the dilatometric experiment of heating sample from ambient temperature to 1050ºC at heating rate of 2ºC/min which allows to determine $Ac_{1s}$ (start of eutectoid transformation) and $Ac_{1f}$ (finish of eutectoid transformation). Ms temperature were determined from the dilatometric test of austenitizing at 900ºC with subsequent cooling to ambient temperature at cooling rate of 50ºC/s (figure 3.4).

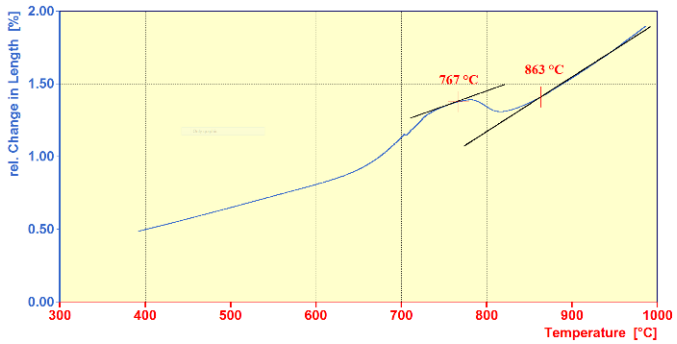


Fig. 3.3. Dilatometric diagram for the tested Mo-Ni-Cu cast iron

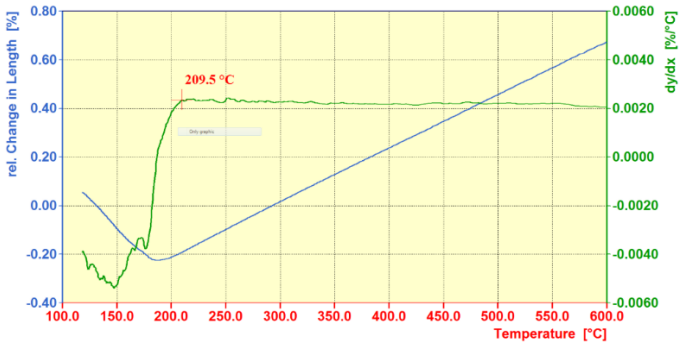


Fig. 3.4. Dilatometric diagram for the tested Mo-Ni-Cu cast iron shows $M_S$ temperature

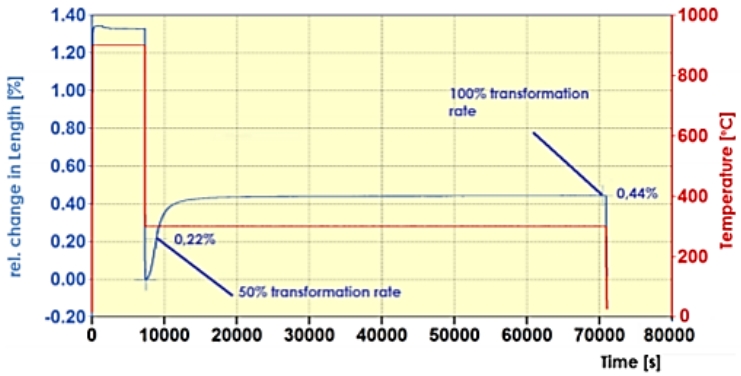


Fig. 3.5. Dilatometric diagram for the tested Mo-Ni-Cu cast iron shows ausferritic-transformation at 300°C

The aim of treatment was maximum refinement of microstructure while avoiding proeutectoid ferrite. Designed process was consisted of double austempering with first auferritic transformation stopped at 50% rate (figure 3.6). Time to 50% of ausferritic transformation at given temperature was determined through dilatometric experiment. Assuming that carbides precipitation during isothermal hold at ausferritic transformation temperature is supressed or negligible due to silicon content, change of length during that hold can be associated solely with austenite to bainitic ferrite transformation. Hence, a given percentage of sample's total length increment corresponds with same percentage of transformation progress (figure 3.5) Immediately after obtaining 50% of transformation material were partially austenitized within intercritical zone and austempered at low temperature for a time sufficient to close processing window. The maximum refinement of the ductile iron matrix microstructure was assumed by selecting a low temperature of isothermal transformation, i.e. 40°C above MS in the bottom bainite range. On the basis of dilatometric plots (Fig. 3.3 and Fig. 3.4) the temperature of 250°C were determined (for 20 hours to complete the 100% ausferrite transformation).

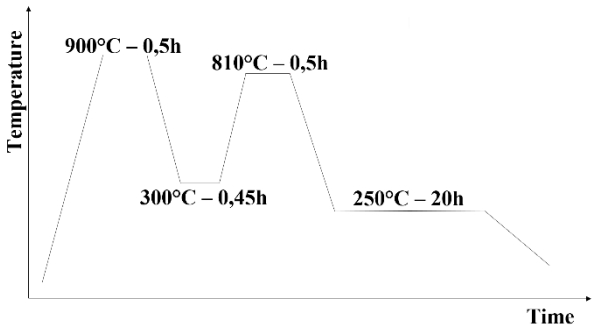


Fig. 3.6. Schemes of conducted heat treatment process of Mo-Ni-Cu ductile iron

## 3. Results and discussion

### 3.1. Microstructure

Figure 3.7-8 shows the obtained cast iron microstructure after heat treatment of dilatometric and bulk samples.

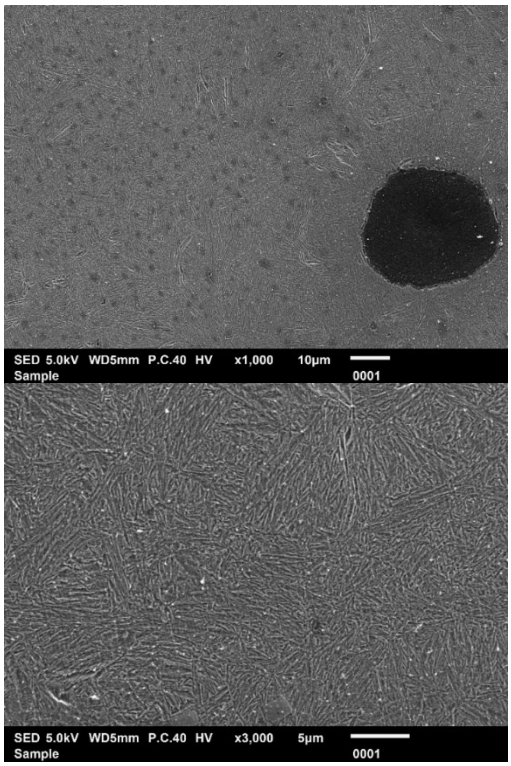

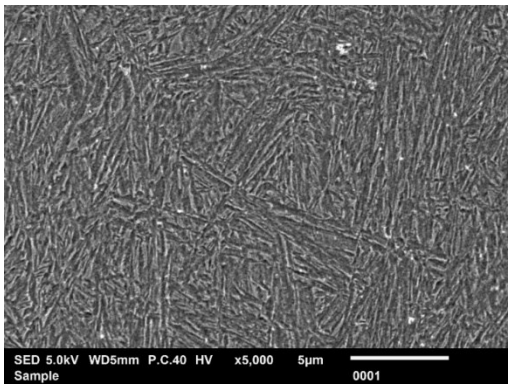


Fig. 3.7. Microstructure of tested dilatometric samples of cast iron after heat treatment (etched with 3% nital)

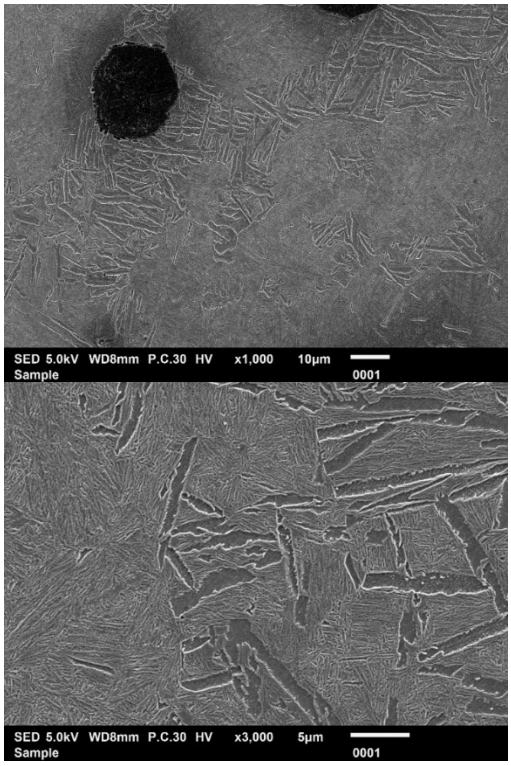

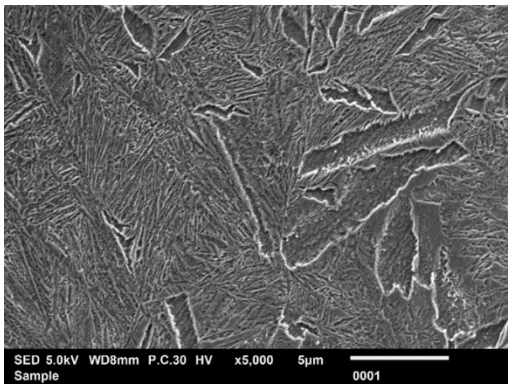


Fig. 3.8. Microstructure of tested metallography samples of cast iron after heat treatment (etched with 3% nital)

The metallographic analysis indicates refinement of the matrix microstructure of the ductile iron after applied heat treatment process within the zone of intercritical heating. The microstructure of both dilatometric and regular samples after heat treatment is characterized by a bainitic matrix. Dilatometric samples featured a uniform microstructure refinement (figure 3.7), while in the case of regular samples large laths of ferrite were also observed (figure 3.8).

Occurrence of large ferrite was distinctive for areas of variable chemical composition in a non-homogeneous matrix of nodular iron. Their formation may be associated with greater thermal inertia comparing to dilatometer samples. However, these plates constitute a small percentage of the matrix microstructure while most of observed ausferrite was characterized by grain refinement even below 100 nm. This gives grounds for concluding that the ausferritic transformation at a respectively low intercritical temperature and prior heat treatment allows the formation of a nanostructured ausferrite matrix of a ductile iron

### 3.2. Hardness and impact tests

Table 3.2 and 3.3 present the obtained results from hardness and impact measurements, in the form of mean values from the measurement along with the standard deviation. Two different loads during the hardness test, smaller 0.2kG and larger-1kG were used to illustrate the difference between matrix and whole material. Hardness results indicate a higher hardness value for dilatometer samples. Difference in HV0.2 hardness between dilatometric and metallographic sample was about 20%. This results from the matrix microstructure after heat treatment processes. Presence of large ferrite plates observed in metallographic samples was the cause of hardness decrement. Furthermore, measured hardness

of the material can be associated with other properties, like tensile strength, due to developed database (figure 3.9).

Table 3.2. Average hardness values for heat treatment of Mo-Ni-Cu cast iron

| | $HV_{1kg}$ (HB) | $HV_{200g}$ |
|---|---|---|
| Regular sample | 485±48 (460) | 500±48 |
| Dilatometric sample | 552±54 (532) | 622±23 |

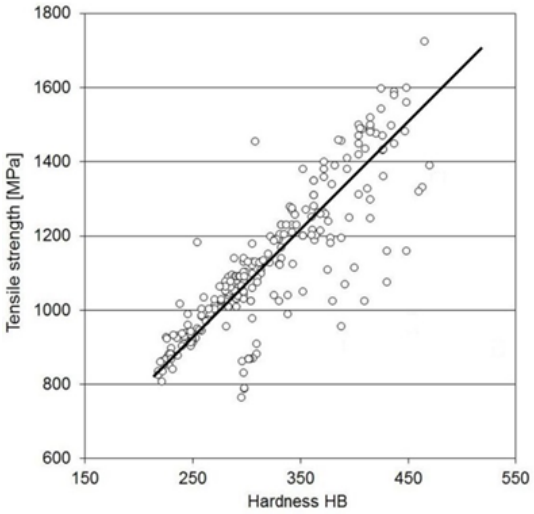


Fig. 3.9. Dependence of tensile strength on HB hardness for ausferritic ductile iron; base on own data

The average impact value for the tested ductile iron is approximately 45 [J] (table 3.3), which should be considered as a good result compared to ADI obtained after conventional heat treatment. Similar studies by the authors described in [6] confirm that reheating of ductile iron above the A1 temperature after the first austempering allows to achieve high impact values.

Table 3.3. Average toughness values for heat treatment of Mo-Ni-Cu cast iron

| Number of measurement | K [J] |
|---|---|
| 1 | 52,8 |
| 2 | 34,3 |
| 3 | 47,6 |
| Average | 45,0 ±9,5 |

## 4. Summary

Obtained results show that proposed heat treatment of ductile iron, consisting double austempering with intercritical austenitization can produce very fine microstructure. A careful design of specific time-temperature parameters of prior austempering ensures uniform distribution of alloying elements within the matrix. Secondary austenitization in the intercritical zone resulted in partial bainitic ferrite to austenite transformation and more even carbon distribution which provided greater nucleation rate of bainitic ferrite during second austempering. Small but significant amount of proeutectoid ferrite was also observed in bulk samples; its location in matrix microstructure suggests it formed in areas of microsegregation of alloying elements. Absence of proeutectoid ferrite in dilatometric samples was probably caused by greater austenitization time to cross section ratio than in bulk samples. Greater volume of latter would require significantly longer austenitization time to achieve similar effect like in dilatometric samples. Good mechanical properties of investigated ductile iron after double austempering indicate considerable potential for new discoveries in the field of strong microstructure fragmentation through cyclic thermal interactions.

## Acknowledgments

This work was supported by the National Centre for Research and Development NCBiR project no PBS3/B5/45/2015.

## References

[1] Artola, G., Gallastegi, J., Izaga, J. (2017). Austempered Ductile Iron (ADI) Alternative Material for High Performance Applications. International Journal of Metalcasting. 11(1), 131–135. DOI: 10.1007/s40962-016-0085-8.

[2] Kobayashi, T., Yamada, S. (1996). Effect of holding time in the (α+γ) temperature range on toughness of specially austempered ductile iron. Metallurgical and Materials Transactions A, 27(7), 1961-1971. DOI: 10.1007/BF02651945.

[3] Putatunda, S.K., Panneerselvam, S., Alshwigi, M. (2015). Development of nanostructured austempered ductile cast iron (ADI). 28th ASM heat treating society conference. 20-22 October 2015. Detroit, USA; ASM International.

[4] Kim, Y., Shin, H., Park, H., Lim, J.D. (2008). Investigation into mechanical properties of austempered ductile cast iron (ADI) in accordance with austempering temperature, Materials Letters, 62, 357–360. DOI: 10.1016/j.matlet.2007.05.028.
[5] Jianghuai, Y., Putatunda, S.K. (2004). Influence of a novel two-step austempering process on the strainhardening behaviour of austempered ductile cast iron (ADI). Materials Science and Engineering A, 382, 256-279. DOI: 10.1016/j.msea.2004.04.076.
[6] Mahmoud, F.H. (2010). Effect of second step austempering temperature and time on the impact properties of twostep austempered SG-cast iron, Journal of Al Azhar University Engineering Sector, 5(14), 59-65.
[7] Aristizabal, R., Foley, R., Druschitz, A.(2012). Inter Metalcast (Intercritically Austenitized Quenched and Tempered Ductile Iron. International Journal of Metalcasting, 6(4) , 7–14. DOI: 10.1007/BF03355534.
[8] Nawrocki, P., Wasiluk, K., Łukasik, K., Myszka, D. (2018). Influence of pre-heat treatment on mechanical properties of austempered ductile cast iron, Archives of Foundry Engineering, Komisja Odlewnictwa Polskiej Akademii Nauk Odddział w Katowicach, 18(1), 176-180. DOI: 10.24425/118833.
[9] Chen, J.K., Tsai, J.S., Chen, B.T. (2011). Toughening of ADI austenitized in intercritical region, TMS-The Minerals, Metals and Materials Society, 3, 701-708. DOI: 10.1002/9781118062173.ch89
[10] Aristizabal, R., Foley, R., Druschitz, A. (2010). Intercriticaly austenitized quenched and tempered ductile iron, International Journal of Metalcasting, 7-14.

**Chapter 4.**

**Adam KURZAWA**[1*]
**Jacek W. KACZMAR**[1]

# STRUCTURE OF THE HOT ROLLED COMPOSITE MATERIALS MANUFACTURED OF EN AW-2024 MATRIX ALLOY WITH $\alpha$-$AL_2O_3$ PARTICLES

The paper presents the results of research of the structures of composite materials manufactured by the pressure infiltration method (*squeeze casting*) of ceramic preforms before and after plastic deformation process realized by hot rolling. Casting of the composite materials was carried out applying the liquid EN AW-2024 matrix alloy, which was reinforced with the preforms made of aluminum oxide $\alpha$-$Al_2O_3$ particles. The ceramic preforms are characterized by the cellular structure, and manufactured composite materials after the infiltration process with liquid EN AW-2024 Al alloy show the structure with clusters of the ceramic, reinforcing particles. The composite materials were subjected to a hot deformation process realized by rolling. The microstructure observations of the hot rolled composite materials were carried out applying the light and scanning microscopy. The microscopic observations confirmed the positive effect of plastic forming on the increase of density realized by hot rolling, which caused the diminishing and removal of the residual porosity left after incomplete infiltration process of ceramic preforms. During the plastic deformation of composite materials due to the transport of particles in the plastic matrix, the uniformity of their arrangement is improved, and the breakdown of agglomerates and clusters of the particles is visible. During the applied plastic deformation, the areas of the matrix free from particles are subjected to much greater deformation in comparison with areas which were rich in ceramic particles, what resulted in the formation of a band structure.
**Keywords:** composite materials, ceramic preforms, plastic forming, pressure infiltration

## 1. Introduction

Composite materials are manufactured by pressure infiltration (*squeeze casting*) of porous ceramic preforms made of particles or fibers characterized usually by the homogeneous structure providing good mechanical and applied

[1]Wrocław University of Technology, Faculty of Mechanical Engineering, Department of Foundry Engineering, Plastics and Automation, Smoluchowskiego 25, 50-372 Wrocław, tel. 71 320 42 35,
[*]e-mail: adam.kurzawa@pwr.edu.pl

properties [1-4]. On the one hand normally applied casting alloys of Al-Si type are characterized by good castability and does not cause problems with proper infiltration of the narrow, often micrometric sizes of the spaces in the porous preforms. On the other hand, the application of Al-alloys normally applied for plastic forming due to their limited castability may cause difficulties in infiltration process [5].

As the result of the infiltration of porous preforms with the Al alloys for plastic forming (Al alloy EN AW-2024), the increased porosity after squeeze casting is ascertained, even if larger squeeze casting pressure is applied. Increased porosity is mainly present in the regions of the ceramic particle's agglomerates, at the interface matrix-reinforcing particles and at the interdendritic spaces of the matrix alloy. The porosity effects on the lowering of the mechanical properties due to the weakening of the bonding at the interface's matrix-strengthening particles. Moreover, the melting of these alloys and the liquid alloy pressing considerably effects on the structure morphology and effects on the segregation of the alloying elements mainly at the grain boundaries.

Nowadays the manufacturing of the new materials is based on the different technologies (hybrid technologies) joined in the one manufacturing process like for instance the powder metallurgical manufacturing of porous ceramic preforms and then the pressure infiltration of porous preforms followed by the plastic forming [6-8]. The expected results of the applied hybrid manufacturing process are connected with the lowering of the porosity, relatively homogeneous distribution of the strengthening elements, relatively small grain size of the cast elements which effects on the increasing of the mechanical properties such as Young modulus, hardness, elongation and compressive strength [9-10]. The plastic forming of composite materials containing strengthening elements like ceramic fibers or particles is connected with the application of larger energy than in the case of the non-reinforced materials [11-12]. According to that phenomenon there is conducted the research on the modelling of the plastic deformation of the composite materials reflecting the stress state in the matrices, inside reinforcing particles and at the interface's matrix-strengthening particles.
The goal of the performed modelling experiments is to point out the optimal parameters of the plastic forming process for the composite materials containing different contents of the strengthening elements (fibers, particles).
In this work the effect of hot plastic working realized by hot rolling of composite materials on EN AW-2024 matrix strengthened with ceramic particles $\alpha$-$Al_2O_3$ on their structure and porosity is discussed.

## 2. Materials and experimental methods

Materials for the investigations were manufactured by pressure infiltration (*squeeze casting*) of porous ceramic preforms made of $\alpha$-$Al_2O_3$ particles connected with the organic binder. As the matrix the aluminum alloy EN AW-

2024 was applied which is normally used as the materials for the manufacturing of machine elements by plastic working process. The properties of applied matrix materials and strengthening particles are shown at the Table 4.1. The investigations of the chemical composition of delivered rods of EN AW-2024 aluminum alloy in agreement with the EN 573-1 standard were performed applying the spectrometer S1 MiniLab 150 delivered by GNR INDIA.

Table. 4.1 Chemical composition of EN AW-2024 matrix alloy and selected properties of $\alpha$-$Al_2O_3$ reinforcing particles

| **EN AW-2024 matrix** – chemical composition [wt. %] | | | | | | | | |
|---|---|---|---|---|---|---|---|---|
| | Si | Fe | Cu | Mn | Zn | Mg | Cr | Ti |
| Results of spectral analysis | 0,48 | 0,39 | 4,18 | 0,52 | 0,17 | 1,36 | 0,08 | 0,08 |
| Chemical composition according to the EN 573-1 standard | 0,5 max. | 0,5 max. | 3,8-4,9 | 0,3-0,9 | 0,25 | 1,2-1,8 | 0,10 | 0,15 max. |
| Density of EN AW-2024: 2,79 [g/cm$^3$] | | | | | | | | |

| **Reinforcement** – Chemical composition [wt. %] | | | | | | | |
|---|---|---|---|---|---|---|---|
| Chemical composition [wt. %] | $SiO_2$ | $Fe_2O_3$ | $Na_2O$ | CaO | $TiO_2$ | $K_2O$ | $\alpha$-$Al_2O_3$ |
| | < 0,03 | < 0,04 | < 0,19 | < 0,01 | < 0,01 | < 0,01 | > 99 |
| Density: 3,95 [g/cm$^3$], particle size: 3-6 [μm] | | | | | | | |

Composite materials were manufactured applying the following technological parameters:

- liquid metal temperature: 750°C,
- preform temperature: 700°C,
- mould temperature: 350°C,
- pressing punch temperature: 150°C,
- pressing pressure: 90 -100 MPa

Manufactured composite materials are characterized by the homogeneous distribution of the strengthening particles within the non-strengthened microareas of diameter 50-60 μm. This distribution is the result of the preform morphology in which the proper content of ceramic particles is reached by the application of the special agent forming pores. Increasing of the ceramic particles content is connected with the decreasing of the quantity of the agent, what effects on the decreasing of dimensions and number of pores. In the framework of performed investigations the composite materials containing 10, 20, 30 and 40 vol.% of α-$Al_2O_3$ strengthening particles were manufactured. The microstructure of

composite material strengthened with 20 vol.% of $\alpha$-$Al_2O_3$ particles after squeeze casting is shown at the Fig. 4.1.

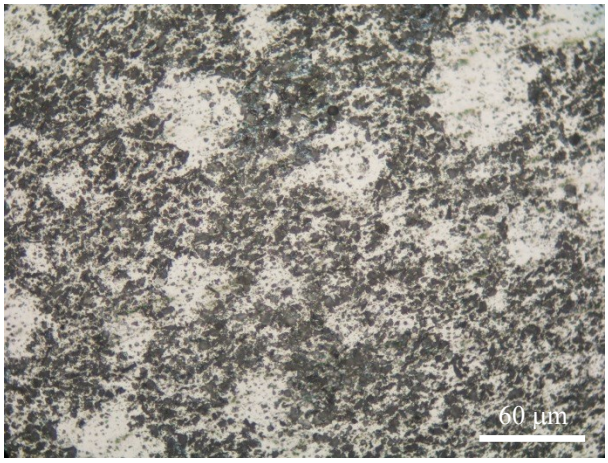


Fig. 4.1. Composite material EN AW 2024+20% vol. of $\alpha$–$Al_2O_3$ particles.

After the infiltration process manufactured composite materials were plastically deformed by hot rolling. The samples for rolling were characterized by the rectangular shape of sizes 60 x 40 x 10 mm. In order to keep the constant temperature during hot working process the sheet pack composed of aluminum EN AW-2024 core and outer steel covers were applied. After each pass the whole pack was heated in order to keep the desired hot rolling temperature. Rolling was performed until the final thickness of aluminum core of 2 mm was achieved, applying in each pass the relative deformation of $\varepsilon$ = 10%. It was ascertained that the processes of the transport of the ceramic particles in the aluminum alloy matrix and the closing of the porosity takes place at the temperature of 500-520$^o$C and final hot rolling process was performed at the temperature of 510 $^o$C.

The structure of manufactured materials was investigated by optical microscopy applying the metallographic microscope NIKIN ME200 and Scanning Electron Microscope Hitachi TM3000. The porosity was investigated applying the Archimedes method applying the analytical balance at the ambient temperature. As the hydrophobic liquid - toluene characterized by the density of $\varrho$ = 0.87 g/cm$^3$ was applied.

## 3. Results and discussion

The limited castability of the EN AW-2024 alloy in comparison to the casting Al-Si alloys causes the difficulties in the pressure infiltration process of microspacies in the ceramic powder preforms. According to that fact in the interdendritic spaces of the matrix and between the agglomerates of ceramic particles the microporosity can occur. With the increasing of ceramic particles content in the composite materials the increase of microporosity is noticed. The general distribution of microporosity is shown at the Fig. 4.2a and distribution of porosity inside particle agglomerates is shown at the Fig. 4.2b.

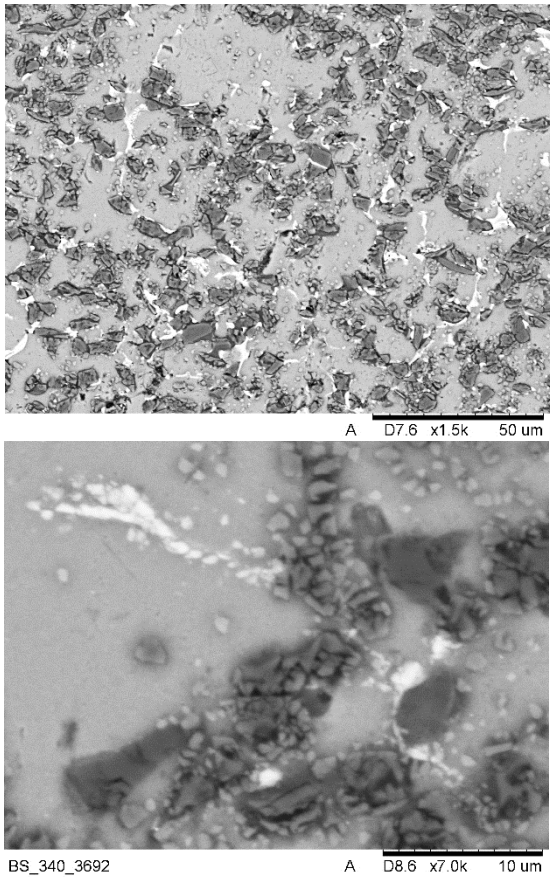


Fig. 4.2. Microstructure of composite material EN AW 2024 – 30% vol. of $\alpha$-$Al_2O_3$ particles manufactured by pressing from liquid state: a) general view, b) porosity inside the particle clusters

The application of hot working causes the deformation of the matrix material which additionally generates the movement of ceramic $\alpha$-$Al_2O_3$ particles in the aluminum alloy matrix. As the result, the closing of the residual porosity and

deformation of micro, non-strengthened regions take place, and these areas becomes relatively long what results in the formation of band structure, similar to the direction of the rolling. The non-reinforced larger microregions were deformed and after the hot rolling process they were characterized by the band structure and part of the smaller non reinforced microregions was plastically deformed and removed. The microstructures of hot rolled materials containing 30 vol.% of ceramic $\alpha$-$Al_2O_3$ particles are shown at the Fig. 4.3. In comparison to the starting materials after squeeze infiltration especially non reinforced microregions were removed.

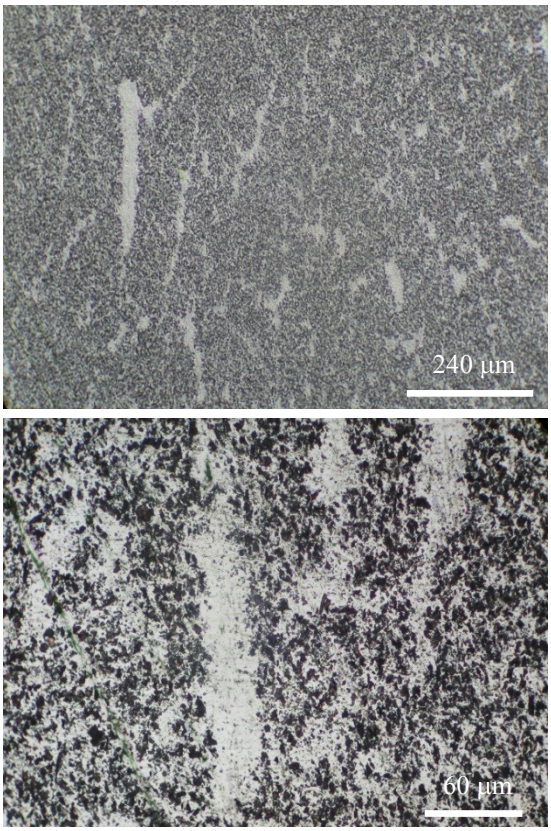


Fig. 4.3. Microstructure of composite material EN AW 2024 – 30% vol. of $\alpha$-$Al_2O_3$ particles subjected to the hot rolling: a) general view b) porosity at region of the particle clusters.

During hot rolling the intermetallic compounds $CuAl_2$ in the EN AW-2024 matrix were deformed, transported in the matrix and there was observed their fragmentation effecting on the improvement of homogeneity of the structure. The

identification of the intermetallic compounds applying the point EDS analysis is shown at Fig. 4.4, and fragmentation of $CuAl_2$ intermetallic compound at the Fig. 4.5.

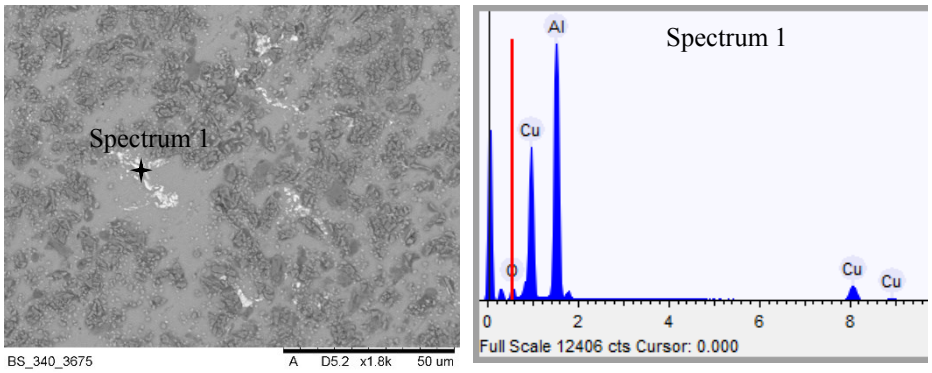


| Element | Weight % | Atomic % |
|---|---|---|
| Aluminum | 54.0 | 73.4 |
| Copper | 46.0 | 26.6 |

Fig. 4.4. EDS analysis: identification of the $CuAl_2$ intermetallic compound in the composite materials EN AW 2024 – 20% vol. of $Al_2O_3$ particles subjected to the hot rolling.

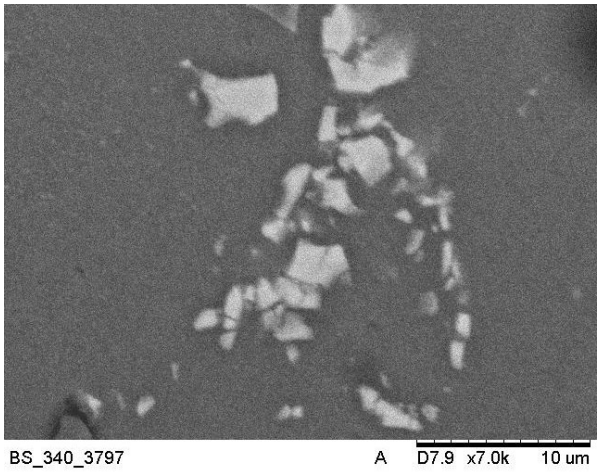


Fig. 4.5. SEM: fragmentation of the $CuAl_2$ intermetallic compounds in composite materials EN AW 2024 – 20% vol. of $Al_2O_3$ ceramic particles after hot rolling.

Measured density which made possible the calculation of porosity showed, that the unreinforced matrix EN AW-2024 alloy after squeeze casting was characterized by the porosity of 1.2%. The porosity of manufactured composite materials increased for larger content of alumina praticles. The relationship between volume content (vol.%) of ceramic particles in the matrix and porosity is shown at the Fig. 4.6.

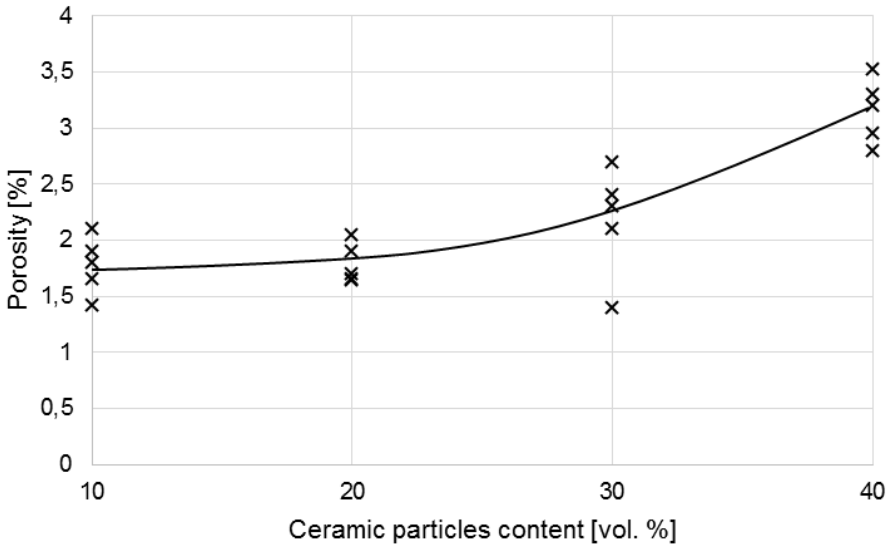


Fig. 4.6. Porosity of the composite materials of EN AW 2024 types – The particles $Al_2O_3$ were manufactured in the infiltration process.

The addition of 10 vol.% and 20 vol.% of ceramic particles effected in 30% increase of porosity, comparing to non-reinforced alloy. The largest porosity of 2.8-3.5 g/cm$^3$ showed composite materials containing 40 vol.% of ceramic particles, what means the 200% increase of porosity comparing to unreinforced alloy.

The plastic working of composite materials by hot rolling at the temperature of T=510$^o$C showed that the porosity is significantly reduced. The largest diminishing of porosity was achieved for samples containing 10 vol.% of ceramic particles and the diminishing of porosity was of 70%. In the composite materials containing 30 vol.% of ceramic particles the reduction of porosity was of 15%. The hot working process by rolling did not effect on the diminishing of porosity in the composite materials containing 40 vol.% of ceramic particles.

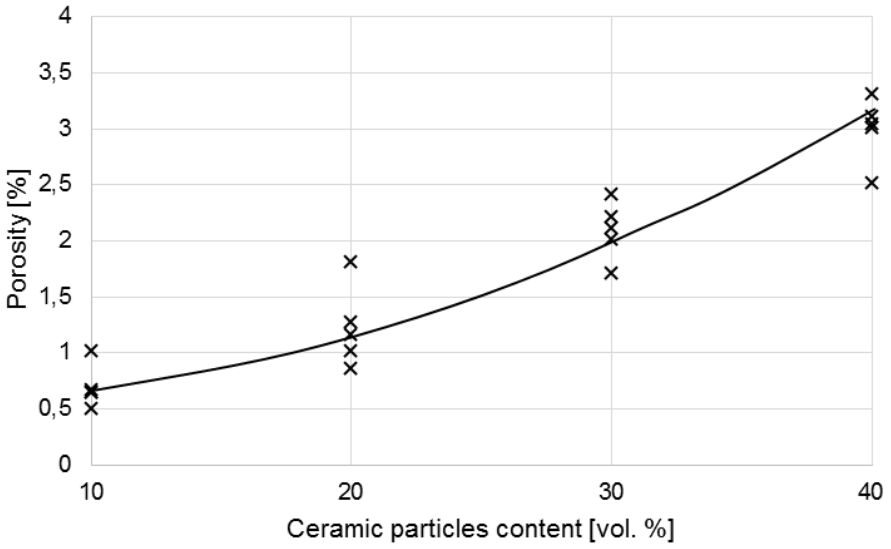


Fig. 4.7. Porosity of the composite materials of EN AW 2024 types – The particles $Al_2O_3$ were manufactured in the infiltration process and subjected to the rolling.

## 4. Conclusions

The application of plastic working by hot rolling considerably effects on the structure of composite materials manufactured by squeeze casting with EN AW-2024 Al alloy of porous preforms from the ceramic particles $\alpha$-$Al_2O_3$. After squeeze casting in the structure of the composite materials are visible ceramic particles with the typical distribution in the form of latticework in the matrix. During hot rolling the typical band structure is generated and the phenomenon of the improvement of homogeneity take place. Moreover, the fragmentation of the $CuAl_2$ intermetallic compounds takes place. The hot rolling process effected on the diminishing of porosity generated during squeeze casting process. The largest decrease of porosity from 1.7% to 0.6% (what means the 65%v reduction of porosity) was achieved for the materials containing 10 vol.% of ceramic particles. The smallest reduction of porosity of 13% after the hot rolling process was noticed for composite materials containing 30 vol.% of particles what can be connected with the negligible plasticity of the matrix comparing to the material strengthened with 10 vol.% of particles. The hot rolling of the composite materials containing 40 vol.% of ceramic particles does not effect of the changes of porosity, what can be connected with the small susceptibility of such composite materials for pores deformation. The transport of the large number of ceramic particles within the matrix containing 40 vol.% of particles is not

possible and the deformation cause the generation of microcracks in these regions and fragmentation of particles. Moreover, the loss of the bonding at the interface ceramic particles-matrix effects on the additional decrease of density.

## References


[1] Venkatesan S., Xavior M. Anthony (2018): Analysis of Mechanical Properties of Aluminum Alloy Metal Matrix Composite by Squeeze Casting – A Review, Materials Today: Proceedings, Vol. 5, Issue 5, Part 2,11175-11184.

[2] Kaczmar J.W. Kurzawa A. (2010): Structure and properties of porous ceramic preforms made of □□alumina particles, Archives of Foundry Engineering 10/1 157-162.

[3] Kumar Subbaraya Mohan, Srinivas S., Ramachandra M., Mahendra K. V. (2018): Characterization of Aluminium Metal Matrix Composite Produced by *Squeeze Casting* Technique, Materials Today: Proceedings, Volume 5, Issue 10, Part 3, 22718-22726.

[4] Prasad K. N. P., Ramachandra M. (2018), Determination of Abrasive Wear Behaviour of Al-Fly ash Metal Matrix *Composites* Produced by Squeeze *Casting*, Materials Today: Proceedings, Volume 5, Issue 1, Part 3, 2844-2853.

[5] Kurzawa A., Kaczmar J.W., Naplocha K. (2018). Właściwości materiałów kompozytowych na osnowie stopu aluminium EN AW-2024 i miedzi, Zeszyty Naukowe Politechniki Rzeszowskiej 298, Mechanika 90, t. XXXV, 90 (3/18), 335-344, DOI: 10.7862/rm.2018.28.

[6] Lokesh, G. N. , Ramachandra, M., Mahendra K. V. (2018): Mechanical and dry sliding wear behaviour of hot rolled hybrid composites produced by direct *squeeze casting* method, Materials Today: Proceedings, Volume 5, Issue 1, Part 3, 2597-2604.

[7] Jian Qin, Zhan Zhang and X-Grant Chen (2017): Mechanical properties and thermal stability of hot-rolled Al–15%B4C composite sheets containing Sc and Zr at elevated temperaturę, Journal of Composite Materials, Vol. 51(18) 2643–2653 DOI: 10.1177/0021998316674351.

[8] Lee J.C., Subramanian K.N. (1995): The tensile properties of hot-rolled (A1203)p-A1 composites, Materials Science and Engineering, A, 196, 71 – 78

[9] Soppa E., Schmauder S., Fischer G., Brollo J., Weber U. (2003): Deformation and damage in Al/$Al_2O_3$, Computational Materials Science, 28, 574–586.

[10] Zhang W.W., Rohatgi P.K.,Shao M., Li Y.Y. (2009): Effect of plastic deformation on microstructure and hardness of 2024/3003 gradient composite ingot prepared by continuous casting, Materials Science and Engineering A 505 120–130.

[11] Xiaopu Li, Chongyu Liu, Kun Luo, Mingzhen Ma, Riping Liu (2016): Hot Deformation Behaviour of SiC/AA6061 Composites Prepared by Spark Plasma Sintering, Journal of Materials Science & Technology 32 291–297

[12] Mahmoud S. Soliman, Magdy M. El Rayes, Adel T. Abbas, Danil Yu. Pimenov, Harri Junaedi (2019),: Effect of tensile strain rate on high-temperature deformation and fracture of rolled Al-15 vol% B4C composite, Materials Science and Engineering: A, Volume 749, 129-136

**Chapter 5.**

**Tomasz MIŁEK**[1*]

# INFLUENCE OF HIGH REDUCTION ON SPREADING FOR VARIABLE INITIAL HEIGHTS OF MATERIAL IN THE EXPERIMENTAL INVESTIGATIONS OF COLD LONGITUDINAL ROLLING OF FLAT BARS MADE FROM EN AW-6063 ALUMINUM

## Abstract

The paper presents experimental results that concern cold longitudinal rolling of flat bars made from EN AW-6063 aluminium alloy. The investigations aimed at determining the impact of the height reduction ($\Delta h$) on the spreading ($\Delta b$) for variable initial heights o material ($h_0$). The samples used in experimental investigations into cold longitudinal rolling were of segments of flat bars having width of $b_0 = 20$ mm, length $l_0 = 40$ mm and different initial heights of $h_0 = 2$ mm; 3 mm; 4 mm and 5 mm, respectively. The longitudinal rolling process is conducted at a special stand – rolling mill DUO-100. The material was rolled with different percent relative rolling reductions (30%; 50%; and 70%, respectively). The theoretical results of spreading calculated from Siebl's, Bachtinov's and Gubkin's formulae were validated against experimental data (Geuze's formula). On the basis o investigations carried out into cold longitudinal rolling of flat bars made from from EN AW-6063 aluminium alloy, it was found that computed and experimental spreading increases with an increase in relative rolling reductions regardless of assumed different initial heights of material.

**Keywords:**
longitudinal rolling, high reduction, spreading, aluminum, EN AW-6063.

---

[1] Department of Metal Science and Materials Technologies, Faculty of Mechatronics and Mechanical Engineering, Kielce University of Technology, al. Tysiąclecia Państwa Polskiego, 25-314 Kielce, Poland
[*] tmatm@tu.kielce.pl

## 1. Introduction

Rolling is the most extensively used metal forming process and it accounts for almost 90% of the metal produced by forming. In this process, the material to be rolled is drawn by means of friction into the gap between two revolving rolls. The rolling process belongs to the compressive deformation processes and has been classified on the basis of kinematics, tool and workpiece geometry. Based on kinematics, the rolling process can be classified as: longitudinal, cross and skewed [1,2]. As can be seen from Fig. 5.1, in longitudinal rolling, the workpiece moves through the rolling gap perpendicular to the axis of the rolls, without rotation about the workpiece axis [2]. In addition to the conventional methods of rolling, there are also special methods, as WPM method for example. The most essential features of this method, distinguishing it from other known methods, involve the use of two circular segments as the tools and the adoption of a kinematics that allows one-directional rolling with a symmetrical system of forces relative to the axis of the rolled material. The WPM method of cold rolling allowed forming cylindrical gears, involute splines and other circular profiles [4].

During longitudinal rolling, the crystals get elongated in the rolling direction and the material emerges at a higher speed than it enters. In cold rolling the crystals more or less retain the elongated shape, but in hot rolling they start to reform after coming out of the deformation zone. The rolls exert compressive stresses on some portion of the workpiece in the rolling process. These stresses, in turn, cause stresses in the workpiece, resulting in plastic flow [2].

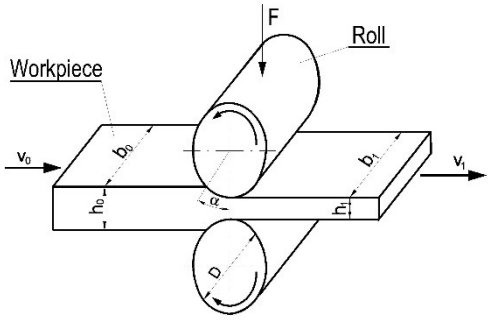


Fig. 5.1. Nomenclature in flat longitudinal rolling [3]

The main phenomena occurring in the deformation zone for rolling include: forward slip, retardation and spreading. Phenomenon like spreading is only occasionally reported in connection with cold longitudinal rolling of aluminum. It is difficult to produce metal flow in the lateral direction in conventional flat rolling process. The spread which occurs during cold flat rolling is expressed as the difference between the width of the section after rolling and before rolling.

Values of spread may be calculated from Geuze's, Siebl's, Bachtinov's and Gubkin's formulae [5,6]. Spread is given by the equation of Geuze below (1) [5,6]:

$$\Delta b = b_1 - b_0 \tag{1}$$

where:
$b_0$ – width of the material before deformation (mm)
$b_1$ – width of the material after deformation (mm)

The following formula can be used to obtain the spread of Sibl theory (2) [5,6]

$$\Delta b_S = a \frac{\Delta h}{h_0} \sqrt{R \Delta h} \tag{2}$$

where:
$h_0$ – height of the material before deformation (mm),
$\Delta h$ – the height reduction (mm),
$R$ – radius of mill rolls (mm),
$a = (0.35 \div 0.45)$ [5,6]

The spread may be estimated from the Bachtinov's formula given below (3) [5,6]:

$$\Delta b_B = 1.15 \frac{\Delta h}{2h_0} \left( \sqrt{R \Delta h - \frac{\Delta h}{2\mu}} \right) \tag{3}$$

where:
$\mu$ – the friction coefficient is (4) [5]:

$$\mu = \sqrt{\frac{1}{\left(1 - \frac{\Delta h_{\max}}{D}\right)} - 1} \tag{4}$$

where:
$\Delta h_{max}$ – the height reduction for maximum deformation.

Spread is given by the equation of Gubkin below (5) [5,6]:

$$\Delta b_G = \left(1 + \frac{\Delta h}{h_0}\right)\left(\mu\sqrt{\Delta h R} - \frac{\Delta h}{2}\right)\frac{\Delta h}{h_0} \tag{5}$$

Existing formulae for predicting spread in flat rolling give tolerable results within the limited ranges of conditions for which they were empirically determined. Conditions are commonly encountered in practice, outside the ranges for which the existing formulae were designed, where predicted values differ widely from experimental results for spread [7].

The degree of deformation of materials for rolling are defined in literature [5]. They are given in table 5.1.

Table 5.1. Degrees of deformation of material after rolling [5]

| Relationship is valid for: | height reduction | spreading of flat bar | elongation |
|---|---|---|---|
| Geometrical relationship, mm | $\Delta h = h_0 - h_1$ | $\Delta b = b_1 - b_0$ | $\Delta l = l_1 - l_0$ |
| Relative strain | $\varepsilon_{wh} = \frac{\Delta h}{h_0}$ | $\varepsilon_{wb} = \frac{\Delta b}{b_0}$ | $\varepsilon_{wl} = \frac{\Delta l}{l_0}$ |
| Percent relative strain, % | $G_h = 100\varepsilon_{wh}$ | $G_b = 100\varepsilon_{wb}$ | $G_l = 100\varepsilon_{wl}$ |
| Ratio of strain | $\gamma = \frac{h_1}{h_0}$ | $\beta = \frac{b_1}{b_0}$ | $\lambda = \frac{l_1}{l_0}$ |
| Logarithmic strain | $\varepsilon_h = \ln\gamma$ | $\varepsilon_b = \ln\beta$ | $\varepsilon_l = \ln\lambda$ |

Selected problems of cold longitudinal rolling process of different products made from aluminum and the design of the tooling have been reported in some studies [8-14].

K.J. Soo et al. [8] conducted a series of rolling tests carried out to study the spread of aluminum bars in relation to systematic variations of speed, temperature and apex angle of pass in square-diamond sequences of rolling. They demonstrated that spread was found to be insensitive to speed change but increased with increasing temperature over the ranges of conditions. Based on the experimental data obtained, a spread formula for aluminum rod rolling was proposed [8].

Gjønnes, L. and Andersson B. [9] discussed the main surface features found during cold rolling of initially twin-rolled cast aluminum such as: grooves, gorges, shingles, cross hatches and rolling ridges. Their paper focused on description and interpretation of how selected surface features evolve. In work experiments with model material were performed to test hypothesis of the deformation sequence and mechanisms operating in the roll gap during cold rolling. The experiments with model material were performed on a laboratory

rolling mill where the rolls were made of transparent polymethylmethacrylate (PMMA) [9].

M. Abo - Elkhier [10] described a new method for spread rolling from the literature, in which several portions of strip width were rolled between a roll that has many circumferential grooves and a flat roll. In his work [9], he introduced new modifications in roll profile and numbers of grooves. The advantages of the new modifications he evaluated through rolling of commercially pure aluminum strips. Based experimental data, he demonstrated that a strip of 70 mm wide and 1 mm thickness have been widened by up to 3.1% for a reduction of 35% .A special purpose nonlinear finite element program has been developed to deal with continuous change of contact between the roll and the strip in each rolling pass. The calculated strain tensor was utilized to investigate the localized necking [10].

Simões F.et al [11] conducted investigations into rolling of 1050-O aluminum alloy. In their work 1050-O aluminum alloy sheets were asymmetrically rolled and annealed. The shear texture obtained is found to be retained after annealing. The improvements of the mechanical response and the texture evolution after heat treatment processing are inferred based on experimental shear tests and numerical simulations. From the results of their analysis it is clear that it is difficult to spread shear texture through the entire sheet thickness from a general asymmetric rolling process

Paper of Ściężor W. et al. [12] presented results of cold rolling strain dependency on the mechanical properties of tested aluminum alloys from 1XXX, 3XXX and 8XXX series, produced in the laboratory conditions with the use of twin roll casting method (TRC) method. In TRC method liquid metal flows into the area formed by two water-cooled rolls, solidifies and next is deformed (rolled) which allows to obtain strip with several millimeters thickness. They demonstrated that thanks to this, it is possible to eliminate hot rolling stage from the typical production technology, and directly subject obtained sheets to cold rolling process.

In their paper, O. Engler et al. [13] discussed the status of the process and materials development of Al-TRB (flexible rolling of aluminum alloy sheet) the prospective of the future development. Considering work-hardening AA 5xxx series and age-hardening AA 6xxx series alloys for automotive applications, they conducted lab-scale experiments in order to elucidate the range of properties which can be realized through flexible rolling while maintaining reproducible constant materials properties according to specification. Large-scale trials were performed to demonstrate that the manufacturing of Al-TRBs is feasible, in that these alloys can be processed in industrial scale to provide homogeneous materials properties over the relevant thickness range for automotive applications.

Grydin O. et al. [14] examined the possibility of producing of flat aluminum strips with tailored mechanical properties across their width by means of rolling. The aim of their the work was an experimental analysis of the effect of cold rolling of the strips with a pre-profiled cross-section in flat rolls. The performed tensile tests and hardness measurements proved the possibility of setting of tailored properties in flat strips by means of rolling. They demonstrated that the difference between the mechanical characteristics of various strip's elements for the selected aluminum alloy can reach 40%.

The paper presents experimental results that concern cold longitudinal rolling of flat bars made from EN AW-6063 alloy aluminum. The investigations aimed at determining the impact of the high reduction ($\Delta h$) on the spreading ($\Delta b$) for variable initial heights of material ($h_0$). The spreading was calculated Geuze's Siebl's, Bachtinov's and Gubkin's formulae (1), (2), (3), (5). The material was rolled with different percent relative rolling reductions ($G_h$ = 30%; 50%; and 70%, respectively).

## 2. Methodology

The material for experimental investigations into cold longitudinal rolling process were samples made from flat bars of EN AW-6063 alloy aluminum. The chemical composition of material [15] are shown in table 5.2. EN AW-6063 alloy aluminum was selected as the testing material in these investigations due to its good formability and wide applications in industry [16-17].

Table 5.2. The chemical composition of EN AW-6063 alloy aluminum [%] [15]

| *Mg* | *Si* | *Fe* | *Ti* | *Zn* | *Cr* |
|---|---|---|---|---|---|
| 0.45 - 0.9 | 0.20 - 0.6 | max. 0.35 | max. 0.10 | max. 0.10 | max. 0.10 |
| *Mn* | *Cu* | *Unspecified other elements* | | | *Al minimum* |
| max. 0.10 | max. 0.10 | Each max. 0.05 | Total max. 0.15 | | rem |

The samples used in experimental investigations into cold longitudinal rolling were of segments having the width of $b_0 = 20$ mm, length $l_0 = 40$ mm and different heights of $h_0 = 5$ mm, $h_0 = 4$ mm, $h_0 = 3$ mm, $h_0 = 2$ mm, respectively. The specimens with heights of $h_0 = 4$ mm, $h_0 = 3$ mm, $h_0 = 2$ mm were obtained by milling from flat bar with height of $h_0 = 5$ mm.

Table 5.3 presents the mechanical properties of the samples of aluminum used in the testing of longitudinal rolling [3]. The properties were determined experimentally by static tensile testing. Tensile test was conducted on *LabTest5.20SP1* testing machine (*LABORTECH* firm) with 20 kN force. Machine was calibrated by PN-EN ISO 7500-1:2005 and meets the metrological requirements for class 0.5.

Table 5.3. The mechanical properties of aluminum EN AW-6063 [3]

| $R_m$ , MPa | $A_{11.3}$ , % | $Z$,% |
|---|---|---|
| 260 | 13.8 | 11.2 |

The longitudinal rolling process is conducted at DUO-100 laboratory rolling mill. It is primarily intended for cold rolling non-ferrous metals. The rolling mill has two mill rolls at diameter D equals 102 mm [18]. Figure 5.2 presents diagram of laboratory stand for cold longitudinal rolling and Figure 5.3 shows view of its main part.

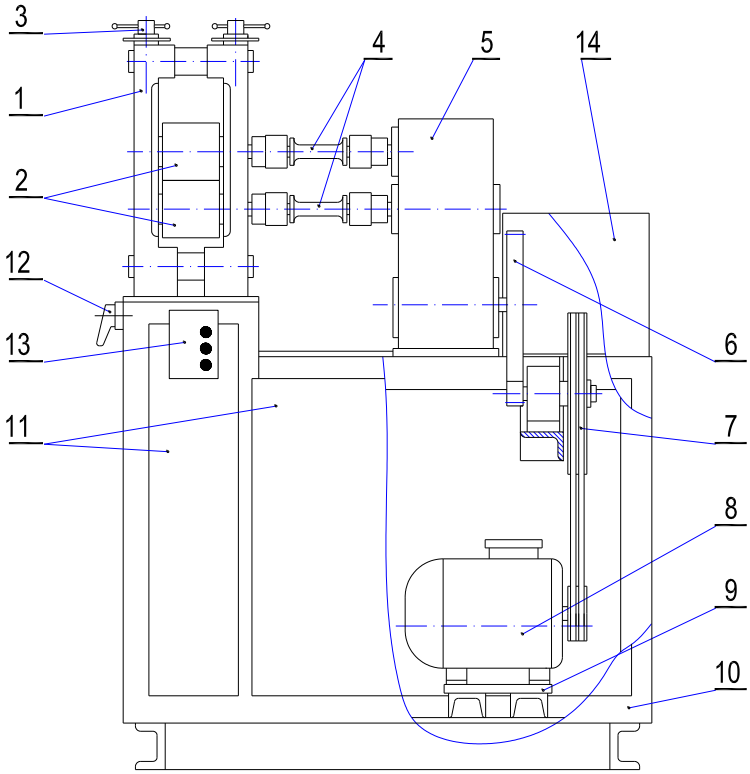


Fig. 5.2. Laboratory stand for rolling – DUO-100 longitudinal rolling mill, where:
1- mill stand, 2- mill roll, 3 – roll positioning mechanism, 4 – mill spindle, 5 – tootheding cage, 6 – toothed gear, 7 – belt transmission, 8 – electric motor, 9 – motor base, 10 – mill housing, 11 – shields of mill housing, 12 - master switch 13 – control, 14 – shield of power feed [18].

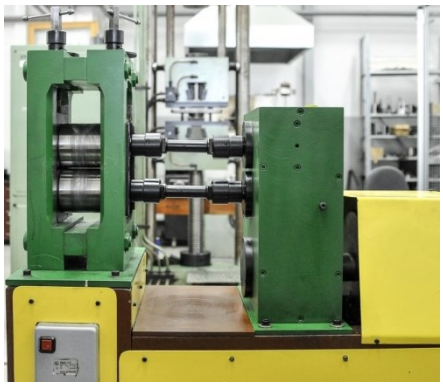

Fig. 5.3. View of the main part of DUO-100 longitudinal rolling mill

The samples were rolled by using extraction naphtha as lubricant. Extraction naphtha is a complex mixture of hydrocarbons obtained by treatment of petroleum fraction with hydrogen in the presence of a catalyst. It is applied to production of adhesives. Extraction naphtha is used to cleaning and degreasing in dry cleaners and tanneries as well as in service workshop. Its density at 15 $^0$C is from 0,62 to 0,88 g/cm$^3$ [19].

## 3. Results and analysis

Each sample at the same height of $h_0$ was rolled with percent relative rolling reductions: 30%; 50%; and 70%, respectively. The measurements of geometric parameters of specimens before and after deformation were taken with micrometer screw, the measuring accuracy of which was up to 0.01 mm (each sample was measured three times and the arithmetic mean was computed).

On the basis of measurements, the values of spreads were calculated by means of Geuze's, Siebl's, Bachtinov's and Gubkin's formulae (1), (2), (3), (5). Table 5.4 presents results of calculations (columns 4÷7).

The friction factor used in Bachtinov's and Gubkin's formulae, was determined by method of the roll bite angle. This method involves rolling samples at maximum degree of deformation. On the basis of geometric parameters of samples after deformation measurements, the value of friction factor ($\mu$ =0.29) were calculated from formula (4).

Values of spreadings calculated by means of Geuze's Siebl's, Bachtinov's and Gubkin's formulae (columns 4÷7 in Table 5.4) increases with increase initial heights o material at the same degree of deformation of material (percent relative rolling reductions).

Influence of the height reduction ($\Delta$h) and the relative strain ($\varepsilon_{wh}$) on the spreading ($\Delta$b) calculated from Geuze's formula (1) for different initial heights

of flat bars made from aluminum EN AW-6063 are shown in diagrams (in Fig. 5.4 and Fig. 5.5, respectively).

Table 5.4. The results of calculations of spreads

| $h_0$, mm | $G_h$, % | $\Delta h$, mm | $\Delta b$, mm formula (1) | $\Delta b_S$, mm formula (2) | $\Delta b_B$, mm formula (3) | $\Delta b_G$, mm formula (5) |
|---|---|---|---|---|---|---|
| *1* | *2* | *3* | *4* | *5* | *6* | *7* |
| 5 | 30 | 1.5 | 0.48 | 0.92 | 1.48 | 0.70 |
| | 50 | 2.5 | 1.13 | 1.97 | 3.19 | 1.52 |
| | 70 | 3.5 | 1.76 | 3.27 | 5.28 | 2.52 |
| 4 | 30 | 1.2 | 0.41 | 0.82 | 1.33 | 0.65 |
| | 50 | 2 | 1.13 | 1.77 | 2.85 | 1.45 |
| | 70 | 2.8 | 1.15 | 2.93 | 4.73 | 2.46 |
| 3 | 30 | 0.9 | 0.48 | 0.71 | 1.15 | 0.59 |
| | 50 | 1.5 | 1.24 | 1.53 | 2.47 | 1.34 |
| | 70 | 2.1 | 1.28 | 2.53 | 4.09 | 2.32 |
| 2 | 30 | 0.6 | 0.22 | 0.58 | 0.94 | 0.51 |
| | 50 | 1 | 0.47 | 1.25 | 2.02 | 1.18 |
| | 70 | 1.4 | 1.01 | 2.07 | 3.34 | 2.08 |

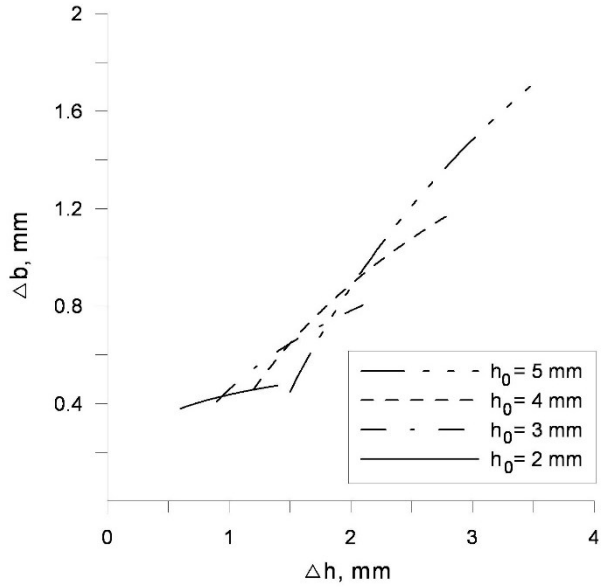


Fig. 5.4. Effect of the height reduction (Δh) on the spreading (Δb) calculated from Geuze's formula for different initial heights of flat bars made from aluminum EN AW-6063

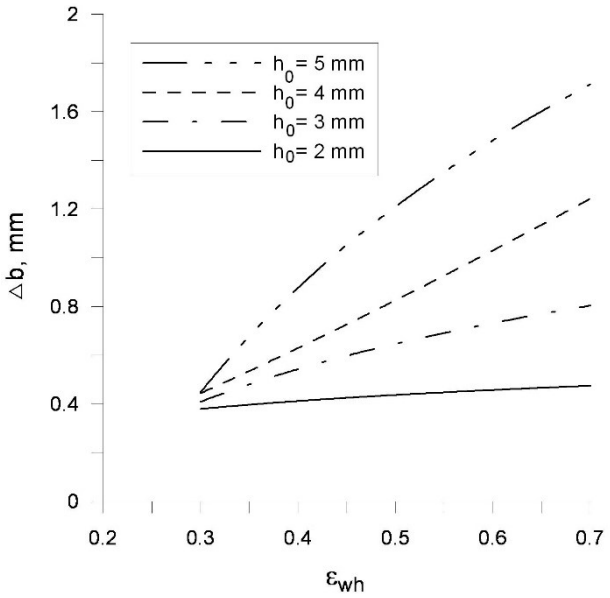


Fig. 5.5. Effect of the relative strain ($\varepsilon_{wh}$) on the spreading calculated from Geuze's formula for different initial heights of flat bars made from aluminum EN AW-6063

Influence of the height reduction ($\Delta h$) on the spreadings ($\Delta b$) calculated from different formulae for the same selected initial height ($h_0$ = 5 mm) of flat bars made from aluminum EN AW-6063 is presented in Figure 5.6. Having compared values of spreadings calculated by means of Geuze's formula (experimental spread) and Siebl's, Bachtinov's and Gubkin's formulae (theoretical spreads), the smallest differences were noted for spreading obtained from Gubkin's formula (Table 5.4 and Fig. 5.6).

The differences between the values of spreadings calculated by means of Geuze's formula and Gubkin's formula did not exceed 45% at $h_0$ = 5 mm (Fig. 5.6). The greatest differences between the values of spreadings calculated by means of Geuze's formula and Bachtinov's formula were noted.

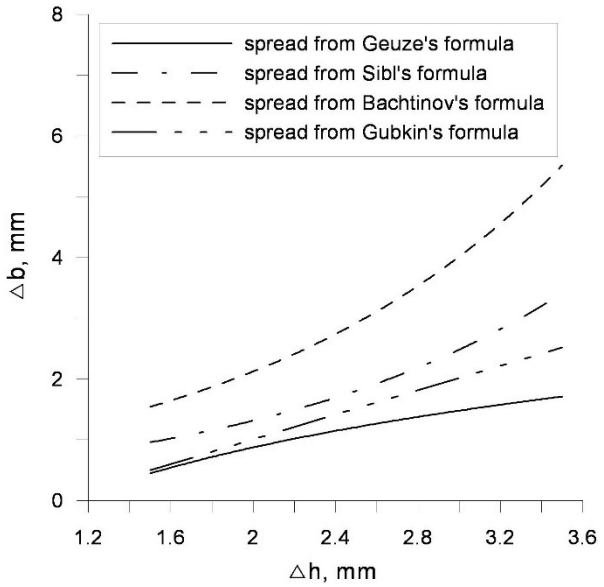


Fig. 5.6. Influence of the height reduction (Δh) on the spreadings (Δb) calculated from different formulae for $h_0$ = 5 mm initial height of flat bars made from aluminum EN AW-6063

## 4. Conclusions

On the basis of investigations carried out into cold longitudinal rolling of flat bars made from EN AW-6063 alloy aluminum (extraction naphtha as a lubricant of rolls), it can be stated as follows:

1. Calculated spread in all cases (Geuze's Siebl's, Bachtinov's and Gubkin's formulae) increases with an increase in height reduction and relative strain for variable initial heights o material.
2. Values of spreadings calculated by means of Geuze's Siebl's, Bachtinov's and Gubkin's formulae (1), (2), (3), (5) increases with increase initial heights o material at the same degree of deformation of material (percent relative rolling reductions).
3. In all cases considered values of spreading were greatest for Bachtinov's formula (3), whereas the lowest values were obtained for Geuze's formula (1).

In view of the growing need for more precise information about the rolling process, it was decided that a series of experiments should be made in the future under carefully controlled conditions to elucidate the effect of the various factors governing spread and to recommend a suitable formula for predicting the spread at cold longitudinal rolling of flat bars likely to occur during industrial rolling operations.

## References


[1] Wusatowski Z. (1969). *Fundamentals of rolling.* Śląsk Press, Katowice.

[2] Lange K. (1985). *Handbook of metal forming.* McGraw-Hill Book Company.

[3] Miłek T. (2018). *The effect of degree of deformation on forward slip in experimental research on cold longitudinal rolling of flat bars made from EN AW-6063 aluminium alloy.* Technical Transactions, vol. 12 , pp. 185-191.

[4] Miłek T., Kopacz Z. (2015). *Evaluation of the possibility of diameter reduction in MT 1020 steel tubes by rolling on the WPM-120 cold profile eccentric rolling machine*. In Metal 2015: 24th International Conference On Metallurgy And Materials, 3-5 Jun 2015, (pp. 377-382), Brno, Czech Republic

[5] Sińczak J. et al. (2001). *Metal forming processes.* AKAPIT Press, Cracow (in Polish).

[6] Żaba K., Mamala A. (2011). *Metal forming of non-ferrous metals. Laboratory exercises. Rolling mill practice and drawing industry.* AGH Press, Kraków (in Polish).

[7] Sparling L.G.M. (1961). *Formula for spread in hot flat rolling.* Applied Mechanics Group, vol. 175, no 11, pp. 604-621.

[8] Soo K. J., Hoggart J.S., Whitton P.W. (1975). *Spread of bars in aluminium rod rolling.* International Journal of Mechanical Sciences, vol. 17, issue 7, pp. 435-443.

[9] Gjønnes, L., Andersson B. (1998). *Mechanisms of surface deformation during cold rolling of aluminium.* Journal of Materials Science, vol. 33, pp. 2469-2476.

[10] Abo-Elkhier M. (2002). *A modified method for lateral spread in thin strip rolling.* Journal of Materials Processing Technology, vol. 124, issues 1–2, pp. 77-82.

[11] Simões F. J. P., Alves de Sousa R. J., Grácio J. J. A., Barlat F., Yoon J. W. (2008). *Mechanical behavior of an asymmetrically rolled and annealed 1050-O sheet.* International Journal of Mechanical Sciences, vol. 50, Issue 9, pp. 1372-1380

[12] Ściężor W., Mamala A., Kwaśniewski P. (2015). *Analysis of properties of selected aluminium alloys, obtained by twin roll casting method and subjected to cold rolling process.* Key Engineering Materials, vol. 641, pp. 202-209.

[13] Engler O., Schäfer C., et al. (2016). *Flexible rolling of aluminium alloy sheet—Process optimization and control of materials properties*. Journal of Materials Processing Technology, vol. 229, pp. 139-148.

[14] Grydin O., Bondarenko S., Stolbchenko M., et al. (2016). *Rolling of flat aluminum strips with tailored mechanical properties*. Materials Science Forum, vol. 854, pp. 87-92.

[15] EN 573-3:2013 *The chemical composition and types of plastically deformed products.* Part 3 The chemical composition and types of products. Poland (in Polish)

[16] Hirsch J. (2011). *Aluminium in innovative light-weight car design.* Materials Transactions, vol. 52, pp. 818-824.

[17] Davis J.R. (1993). *Aluminum and Aluminum Alloys.* ASM Specialty Handbook, ASM International, Ohio.

[18] *Technical documentation of DUO-100 rolling mill.* Faculty of Mechatronics and Mechanical Engineering. Kielce University of Technology. Poland (in Polish).

[19] *Safety data sheet of a chemical substance in accordance with Regulation* (UE) no 453/2010. Low-aromatic extraction naphtha. PPHU „Chem-Rozlew", 2013, p. 10. Poland (in Polish).

## Streszczenie

MATERIAL, TECHNOLOGIES, CONSTRUCTIONS: “Special purpose materials” to spójna monografia składająca się z pięciu rozdziałów o tematyce dotyczącej materiałów specjalnego przeznaczenia. W pierwszym rozdziale poruszono tematykę dotyczącą pierwiastków ziem rzadkich stosowanych w przemyśle zbrojeniowym i metalurgicznym. Rozdział drugi obejmuje zagadnienie dotyczące porowatości kompozytów odlewanych nasycanych stopem aluminium. W rozdziale trzecim autorzy przedstawiają zagadnienia z zakresu właściwości mechanicznych żeliwa ADI. Określono wytrzymałość, twardość oraz udarność w zależności od temperatury obróbki cieplnej żeliwa. Rozdział czwarty przedstawia wyniki badań kompozytowego stopu aluminium do przeróbki plastycznej. Przeprowadzono badania porowatości oraz mikrostruktury kompozytu w zależności od zawartości cząstek ceramicznych. Rozdział piąty przedstawia wyniki badań przeróbki plastycznej stopu aluminium podczas walcowania wzdłużnego. Określono zmianę grubości i naprężeń podczas walcowania oraz wzajemnych korelacji tych parametrów.

## Abstract

MATERIAL, TECHNOLOGIES, CONSTRUCTIONS: "Special purpose materials" is a coherent monograph consisting of five chapters on the subject of special purpose materials. The first chapter deals with rare earth elements used in the military and metallurgical industries. The second chapter covers the issue of the porosity of cast composites saturated with an aluminium alloy. In the third chapter the authors present issues concerning mechanical properties of ADI cast iron. Strength, hardness and impact strength were determined depending on the temperature of heat treatment of the cast iron. Chapter four presents the results of tests of composite aluminium alloy for the plastic processing. The porosity and microstructure of the composite depending on the content of ceramic particles were investigated. Chapter 5 presents the results of investigations of the plastic processing of aluminium alloy during longitudinal rolling. The change of thickness and stresses during rolling and mutual correlations of these parameters were determined.